

# The *XMM*-LSS catalogue: X-ray sources and associated multiwavelength data. Version II

L. Chiappetti<sup>1\*</sup>, N. Clerc<sup>2,5</sup>, F. Pacaud<sup>3</sup>, M. Pierre<sup>2</sup>,  
A. Guéguen<sup>2,6</sup>, L. Paioro<sup>1</sup>, M. Polletta<sup>1</sup>, O. Melnyk<sup>4,7</sup>, A. Elyiv<sup>4,8</sup>, J. Surdej<sup>4</sup>, L. Faccioli<sup>2</sup>

<sup>1</sup>INAF, IASF Milano, via Bassini 15, I-20133 Milano, Italy

<sup>2</sup>Laboratoire AIM, CEA/DSM/Irfu/Sap, CEA-Saclay, F-91191 Gif-sur-Yvette Cédex, France

<sup>3</sup>Argelander Institut für Astronomie, Universität Bonn, Auf dem Hügel 71, D-53121 Bonn, Germany

<sup>4</sup>Institut d'Astrophysique et de Géophysique, Université de Liège, Allée du 6 Août, 17, B5C, 4000 Sart Tilman, Belgium

<sup>5</sup>present address: Max-Planck-Institut für extraterrestrische Physik, Giessenbachstraße, D-85748 Garching, Germany

<sup>6</sup>present address: GEPI, Observatoire de Paris, CNRS, Université Paris Diderot, 5, place Jules Janssen, F-92195 Meudon, France

<sup>7</sup>Astronomical Observatory, Kyiv National University, vul. Observatorna 3, 04053 Kyiv, Ukraine

<sup>8</sup>Main Astronomical Observatory, Academy of Sciences of Ukraine, vul. Akademika Zabolotnoho 27, 03680 Kyiv, Ukraine

revised version submitted 2012 October 12; in original form 2012 June 22

## ABSTRACT

We present the final release of the multi-wavelength *XMM*-LSS data set, covering the full survey area of 11.1 square degrees, with X-ray data processed with the latest *XMM*-LSS pipeline version. The present publication supersedes the Pierre et al. (2007) catalogue pertaining to the initial 5 deg<sup>2</sup>. We provide X-ray source lists in the customary energy bands (0.5–2 and 2–10 keV) for a total of 6721 objects in the deep full-exposure catalogue and 5572 in the 10ks-limited one, above a detection likelihood of 15 in at least one band. We also provide a multiwavelength catalogue, cross-correlating our list with IR, NIR, optical and UV catalogues. Customary data products (X-ray FITS images, CFHTLS and SWIRE thumbnail images) are made available together with our interactively queryable database in Milan, while a static snapshot of the catalogues has been supplied to CDS.

**Key words:** catalogues, surveys, X-rays: general

## 1 INTRODUCTION

The rationale for the *XMM*-Large Scale Structure (*XMM*-LSS) survey was presented in Pierre et al. (2004). A first catalogue for the 5.5 deg<sup>2</sup> surveyed until year 2003 was presented in Pierre et al. (2007, hereafter Paper I). In the present paper, we supersede the first release with a new version which covers the entire 11.1 deg<sup>2</sup> area of the survey. All the data were processed or re-processed afresh with the latest version of our pipeline (see Section 3.1). We release two families of X-ray database tables (see Section 2.4), a standard catalogue (termed 2XLSS) for event files truncated to a common uniform exposure of 10 ks, and a *deeper* catalogue (termed 2XLSSd) using the full exposure time.

The *XMM*-LSS survey area, located around  $2^{\text{h}}30^{\text{m}} -5^{\circ}$ , was covered in the optical band by the Canada France Hawaii Telescope Legacy Survey<sup>1</sup> Wide and Deep Synoptic fields (CFHTLS-W1 and D1); in the NIR band partially by the UKIRT Infrared Deep Sky Survey<sup>2</sup> (UKIDSS; Lawrence et al. 2007); in the IR by the *Spitzer*

Wide-area InfraRed Extragalactic survey<sup>3</sup> (SWIRE; Lonsdale et al. 2003); and in the UV by the Galaxy Evolution Explorer<sup>4</sup> (*GALEX*; Martin et al. 2005) all-sky survey. We release also a multiwavelength database table (using data from the sources just described) in conjunction with each of the X-ray table families.

Data from the present catalogue have already been used in other works, published, submitted or in preparation, e.g. Adami et al. (2011), Elyiv et al. (2012), Willis et al. (2012), Melnyk et al. (2012), Clerc et al. (2012b).

The plan of the paper is as follows: in Section 2 we describe the layout and content of our catalogue, in particular Section 2.4 presents our database system by which users can have public access to the entire data tables and associated data products (a reduced summary will be available via the Centre de Données de Strasbourg [CDS<sup>5</sup>]); Section 3 describes the X-ray data processing and Section 4 the generation of the multiwavelength catalogue. Finally some statistics are presented in Section 5, and concluding remarks in Section 6.

\* E-mail: lucio@lambrate.inaf.it

<sup>1</sup> <http://cfht.hawaii.edu/Science/CFHTLS/>

<sup>2</sup> <http://www.ukidss.org/>

<sup>3</sup> <http://swire.ipac.caltech.edu/swire/swire.html>

<sup>4</sup> <http://www.galex.caltech.edu/>

<sup>5</sup> <http://cdsweb.u-strasbg.fr>

**Table 1.** The complete list of *XMM*-LSS pointings in chronological order of observation.

Column (1) in each group of 4 is our own internal *field name* (the letter G refers to the Liège/Milan/Saclay Guaranteed Time, the letter B to Guest Observer time, and the letter S to the SXDS; the suffix a,b,c indicates repetition of a pointing because of insufficient exposure after high background filtering).

Fields flagged *bad* in column (3) have usually been repeated except for B17c, B45b, B47b, B68b which are the latest and best, though nominally bad, and are necessary in order to avoid holes in the covered area.

Column (2) is the ESA ObsId identifier which can be used to look-up to the pointing in the *XMM-Newton* log and archive.

The exposure (in ks) indicated in column (4) is the weighted mean of MOS1, MOS2 and pn nominal exposures. These exposure times refer to 2XLSSd. For 2XLSS all exposures longer than 10 ks have been curtailed to such a length at event file generation time.

(1)	(2)	(3)	(4)	(1)	(2)	(3)	(4)	(1)	(2)	(3)	(4)
S01	011237 0101	†	80.2†	B20	003798 2001		14.9	B49	040496 6301		10.5
S02	011237 0301		37.1	B21	003798 2101		12.6	B51	040496 6501		8.9
S03	011237 0401		15.7	B26	003798 2601		11.3	B52	040496 6601		12.5
S04	011237 1701		45.3	B27	003798 2701		13.8	B54	040496 6801		13.6
G17	011111 0301		20.6	B17a	003798 1701	bad	3.3	B55a	040496 6901	bad	6.6
G18	011111 0401		23.9	B18	003798 1801		13.7	B56	040496 7001		13.5
G13	010952 0501		21.4	B19	003798 1901		10.9	B57	040496 7101		10.5
G19	011111 0501		20.5	G03	011268 0301		20.7	B59	040496 7301		10.7
G15	011111 0101		16.9	B25	003798 2501		8.6	B60	040496 7401		13.5
G16a	011111 0201	bad	3.7	B24	003798 2401		14.0	B61a	040496 7501	bad	6.4
G16b	011111 0701		9.1	B23	003798 2301		7.9	B62	040496 7601		10.4
B01	003798 0101		11.6	B22a	003798 2201	bad	5.1	B63	040496 7701		12.6
B06	003798 0601		10.4	B28	014711 0101		10.4	B64	040496 7801		13.6
B02	003798 0201		10.5	B29	014711 0201		9.5	B65	040496 7901		13.5
B07	003798 0701		9.4	B30	014711 1301		11.4	B66	040496 8001		13.5
B03	003798 0301		10.7	B31	014711 1401		10.0	B67a	040496 8101	bad	4.8
B05	003798 0501		13.4	B32a	014711 1501	bad	1.6	B68a	040496 8201	bad	2.0
B04a	003798 0401	bad	5.9	B42a	040496 5601	bad	10.6	B69	040496 8301		8.7
B09	003798 0901		11.4	B58a	040496 7201	bad	6.0	B70a	040496 8401	bad	4.5
G01	011268 0101		24.2	B44a	040496 5801	bad	5.4	B72	040496 8601		11.8
G04	010952 0101		23.3	B53	040496 6701		9.4	B71	040496 8501		10.8
G10	010952 0201		22.0	B48	040496 6201		9.4	B58b	055391 1401		23.5
G07	011268 1001		22.2	B04b	040496 0101	bad	8.9	B61b	055391 1601		12.2
G09	010952 0601		19.5	B13b	040496 0201	bad	4.8	B70b	055391 1901		10.6
G14	011268 0801		11.0	B17b	040496 0301	bad	6.0	B44b	055391 0901		23.2
G12a	010952 0401	bad	1.7	B32b	040496 0401		10.5	B45b	055391 1001	bad	8.1
G11	010952 0301		19.3	G12b	040496 0501		9.5	B46b	055391 1101		21.1
G05	011268 0401		21.7	B22b	040496 0601		8.8	B04c	055391 0101		10.5
B08	003798 0801		8.7	B33	040496 4701		9.3	B13c	055391 0201		10.6
G02	011268 0201		8.9	B34	040496 4801		9.2	B17c	055391 0301	bad	7.8
B10	003798 1001		10.9	B35a	040496 4901	bad	5.1	B35b	055391 0401		10.0
B11	003798 1101		10.0	B36a	040496 5001	bad	8.1	B47b	055391 1201	bad	6.3
B12	003798 1201		9.4	B37a	040496 5101	bad	8.0	B36b	055391 0501		10.6
B13a	003798 1301	bad	4.4	B38	040496 5201		10.6	B50b	055391 1301		9.7
B14	003798 1401		9.3	B39	040496 5301		10.4	B41b	055391 0701		11.2
G08	011268 0501		19.0	B40	040496 5401		14.2	B42b	055391 0801		12.5
B15	003798 1501		10.3	B41a	040496 5501	bad	4.4	B37b	055391 0601		14.3
B16	003798 1601		10.2	B43	040496 5701		13.4	B55b	055391 1501		12.6
G06	011268 1301		13.4	B45a	040496 5901	bad	6.8	B67b	055391 1701		12.4
S06	011237 0701		46.9	B46a	040496 6001	bad	7.0	B68b	055391 1801	bad	4.9
S07	011237 0801		35.8	B47a	040496 6101	bad	5.9				
S05	011237 0601		32.7	B50a	040496 6401	bad	4.8				

† For field S01 the full exposure is much longer than the typical *XMM*-LSS exposure and for this reason the relevant data are fictitiously flagged bad in 2XLSSd, while those deriving from an analysis curtailed at 40 ks are used instead, with a field name of S01\_40 in column (1) and an exposure of 40.0 ks in column (4).

## 2 CATALOGUE LAYOUT AND CONTENT

### 2.1 List of available pointings

The entire *XMM*-LSS survey consists of 91 positions on the sky arranged with a regular spacing. Some of the pointings were however repeated once or twice, because the first observations were flagged bad due to a too high background or insufficient clean exposure time. A total of 117 pointings were executed during the Guar-

anteed Time, AO-1, AO-2, AO-5 and AO-7 periods. In addition 7 pointings of the independent Subaru *XMM-Newton* Deep Survey (SXDS; Ueda et al. 2008), with a somewhat different spacing but fully surrounded by our own pointings, were retrieved from the archives and reanalysed by us with our pipeline. The complete list of all 124 pointings is given in Table 1, while the layout on the sky is plotted in Fig. 1.

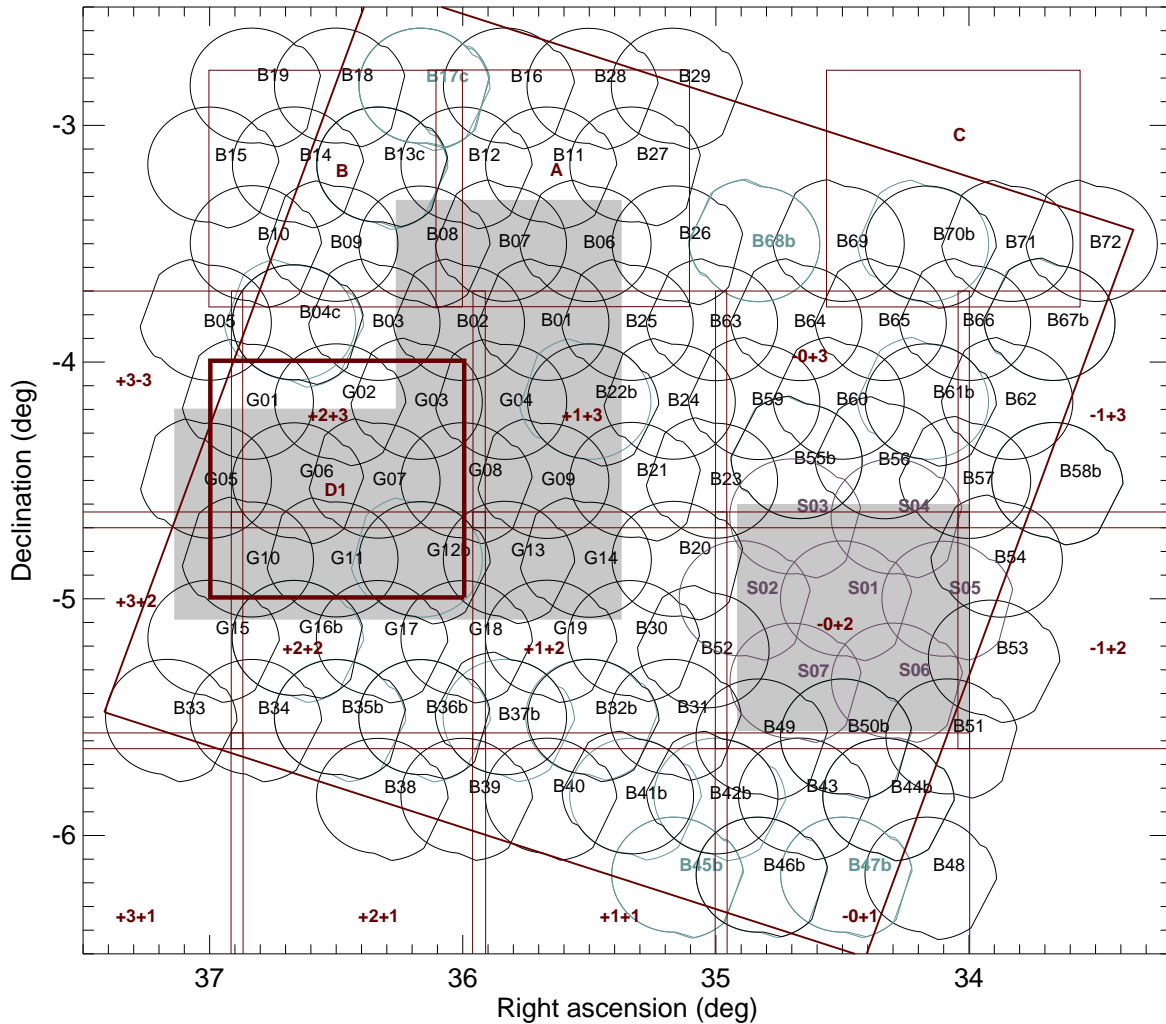


**Figure 1.** Layout of the XMM-LSS pointings and coverage in other wavebands. The position of the XMM FOV footprints of good pointings are plotted and labelled with their field name (in black). SXDS pointings are plotted and labelled in gray (pink-gray in the web version). Bad pointings (later repeated by a good one) are plotted in light gray (blue-gray in the web version), without labels (except for the 4 cases where even the last re-observation is nominally bad). The total geometrical area is estimated to be  $11.1 \text{ deg}^2$ . The dark gray (maroon in the web version) squares indicate the various tiles of the CFHTLS W1 survey (labelled with their short  $\pm x \pm y$  name; see <http://terapix.iap.fr/cplt/oldSite/Descart/cfhtls/cfhtlswidemosaiactargetW1.html>), of our own supplementary pointings (labelled ABC) and the CFHTLS D1 field (thick). The large tilted square is the area covered by the SWIRE survey. The shaded areas are those covered by the UKIDSS surveys (DXS, left; UDS, right) in release DR5. The entire area is covered by the GALEX AIS and DIS surveys.

## 2.2 The X-ray source lists

In this paper we present two variants of the X-ray catalogue, each including source lists for two bands, 0.5–2 and 2–10 keV, named B and CD respectively. The *deep* catalogue (2XLSSd) is obtained from the processing of event files for the entire exposure of each pointing (with the exception of pointing S01, whose duration is much longer than all other pointings, and which has been processed also as a “chunk” of 40 ks). The *standard* catalogue (2XLSS) instead uses a uniform exposure of 10 ks for all pointings longer than that. Both catalogues share an identical processing and the same layout. The list of database columns are reported in Tables A1 and A2 in Appendix A.

## 2.3 The multiwavelength catalogues

We provide also multiwavelength catalogues, named in the database 2XLSSOPT and 2XLSSOPTd (see list of database columns in Table A3 in Appendix A), generated correlating the X-ray source list with optical, NIR, IR and UV catalogues as described in Section 4.

## 2.4 Summary of online availability

### 2.4.1 The database tables

The database site at IASF Milano described in Paper I was relocated since August 2007 to the new site <http://cosmosdb.iasf-milano.inaf.it/XMM-LSS/>, and converted to the DART interface (Paiero et al. 2008) developed by us and used

**Table 2.** The database tables of the current release

Data sets	Tables
10 ks catalogues	
Merged catalogue (all parameters):	2XLSS
Single-band catalogues:	2XLSSB, 2XLSSCD
Multiwavelength catalogue:	2XLSSOPT
deep catalogues	
Merged catalogue (all parameters):	2XLSSd
Single-band catalogues:	2XLSSBd, 2XLSSCDd
Multiwavelength catalogue:	2XLSSOPTd
XMDS catalogues	
Multiband X-ray catalogue:	XMDS
Multiwavelength catalogue:	XMDSOPT

at IASF to support several other projects. While the underlying MySQL database structure is virtually unchanged since the one described in Chiappetti et al. (2005), the user interface has been improved and in particular now requires public users to register with an individual username (see instructions reachable from the home page).

In addition to the material described in Paper I (which will continue to remain available), the database tables listed in Table 2 (plus the data products described in Section 2.4.2) will be available in our database allowing fully interactive selection. Refer to Appendix A for the subset available in electronic form also at CDS.

Single-band tables are provided separately for the B [0.5-2] keV and CD [2-10] keV bands. They contain a selection of parameters generated by XAMIN, like both sets of values computed for the point-like and extended source fit. Position errors and fluxes are derived a posteriori, and computed as per Section 3.1.1. Only sources above a detection likelihood of 15 are made available in the single-band tables. Redundant sources detected in overlapping regions of different pointings are removed as explained in Section 3.4;

The B-CD band merged catalogue is obtained matching single band detections within a correlation radius of  $10''$  (see Section 3.3), and includes only the parameters for the classification (point-like or extended) relative to the *best band*. Data in the other band are made available even if they have a detection likelihood below 15.

#### 2.4.2 Associated data products

Data products are files associated with a given database entry. We distinguish the case of *per-pointing* and *per-object* data products. When a database query returns a number of X-ray sources, each of them may point to an individual data product, or to one common to the pointing where the source was detected. The database interface allows the user to retrieve individual data products, or to build on the fly a `.tar.gz` file containing all the products related to the query.

##### 2.4.2.1 X-ray images

The following X-ray data products are available *per-pointing* for the deep catalogue only:

(i) The B and CD band photon images (one mosaic cumulative for the 3 detectors, after the event filtering)

- (ii) The B and CD wavelet images derived from the above
- (iii) Separate exposure maps for the 3 detectors and 2 bands.
- (iv) ds9 contours (log-spacing based on B band wavelet images)

All images have a pixel size of  $2.5''$ . Note that the World Coordinate System (WCS) of the X-ray images is the one generated by the SAS, therefore it does not take into account the astrometric correction described in Section 3.2. Consequently when overlaying X-ray source positions exactly on the X-ray images, one should use the coordinates labelled as “raw” in Table A1, although this does not make much difference for most of the sources, given the pixel size.

##### 2.4.2.2 Multiwavelength data

The following thumbnail images are available *per X-ray source* in association with the band merged and multiwavelength catalogues (deep version only). The FITS thumbnail images have proper WCS which allows direct overlaying of X-ray astrometrically corrected positions as well as counterpart positions.

(i) FITS CFHT images ( $40'' \times 40''$ ) in the  $i'$  band for sources covered by the CFHTLS W1 or D1 fields and/or in the  $g'$  band when covered by our own ABC fields, obtained via the CADC cutout service<sup>6</sup>. A PNG version is also available as for Paper I.

(ii) FITS SWIRE images in the 4 IRAC bands ( $30'' \times 30''$ ) and in the 3 MIPS bands ( $60'' \times 60''$ ), obtained via the IPAC Gator cutout service<sup>7</sup>

## 3 X-RAY DATA PROCESSING

The original XAMIN pipeline used in Paper I was described in detail in Pacaud et al. (2006). While referring to such papers for detail, we summarize here the main processing steps.

Standard SAS tasks are used to generate event lists. They are filtered for solar soft proton flares and used to produce images for the three EPIC detectors, which are then co-added in each energy band. Such per-band images are filtered in wavelet space, and scanned by a source detection algorithm based on SExtractor (Bertin & Arnouts 1996) to obtain a primary source list. Source characterization is then performed with XAMIN, a maximum likelihood profile fitting procedure, designed for the XMM-LSS survey, optimized for extended X-ray sources and associated signal to noise regimes. XAMIN performs parallel fits with two classes of surface-brightness models, a point-like one and an extended ( $\beta$ -profile) one and outputs the main parameter for both models in a FITS table per pointing and per band. Further processing (as described in Sections 3.2, 3.3 and 3.4) is performed contextually or after ingestion of XAMIN output into our database.

### 3.1 The revised pipeline

For this release, we used the latest version *pro tempore* (3.2) of XAMIN, which has been improved while translating it from IDL to Python (open source). All pointings, including those reported in the XLSS catalogue in Paper I, have been (re)processed afresh with this latest version.

The XAMIN pipeline output parameters for version 3.2 are

<sup>6</sup> <http://www.cadc-ccda.hia-ihp.nrc-cnrc.gc.ca/>

<sup>7</sup> <http://irsa.ipac.caltech.edu>

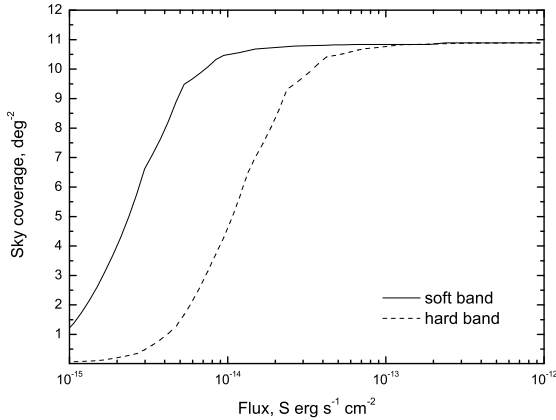


**Figure 2.** Effective sky coverage for the entire *XMM*-LSS area in the soft (B, [0.5-2] keV) and hard (CD, [2-10] keV) bands. This figure, reproduced from Fig. 9 of Elyiv et al. (2012), updates and supersedes Fig. 2 of Paper I. The computation derives from simulations of realistic *XMM*-LSS observations processed by XAMIN.

the same listed in Table 2 of Paper I (and flagged in column (X) in Tables A1 and A2).

The event file generation (and the subsequent pipeline) was applied independently to the full exposure of each pointing, as well as to 10 ks curtailed chunks (from the beginning of the exposure). The latest *XMM* calibrations available *pro tempore* were applied.

One of the differences between the old and new pipeline is the correction of an offset of 0.5 pixel (where our pixel size is 2.5'') in XY image positions. For this reason all X-ray source positions and catalogue names (see Section 3.5) have changed.

We checked that the new pipeline version provides results consistent with the previous IDL version by performing detailed tests on simulated and real *XMM* pointings; then we proceeded to a direct comparison, which shows a (good) agreement between the old and new pipeline as reported in Appendix C1.

This is a summary list of all differences in catalogue generation with respect to Paper I.

- (i) more input data (5 to 11 deg<sup>2</sup>)
- (ii) used latest SAS version and calibrations
- (iii) used XAMIN version 3.2
- (iv) in particular half-pixel offset cured (see above)
- (v) astrometry using CFHTLS T004 (see Section 3.2)
- (vi) band merging at 10'' (see Section 3.3)
- (vii) overlap removal at 10'' (see Section 3.4)
- (viii) web site relocated (see Section 2.4)
- (ix) more multi- $\lambda$  bands (see Section 4)

In addition to the XAMIN output, a number of parameters are calculated a posteriori in order to facilitate the interpretation of the data set. Since in its present state, XAMIN does not perform error calculations, mean statistical errors were estimated by means of extensive simulations, as explained in Paper I and Pacaud et al. (2006); we note that only the first 2 digits are to be considered significant for the count rate and for the core radius as well as for the derived quantities.

Analogously to Paper I, only sources with an off-axis angle < 13' are processed by XAMIN. The catalogues include all the ex-

**Table 3.** The Energy Conversion Factors for the individual EPIC cameras and energy bands, in units of  $10^{-12}$  erg s<sup>-1</sup> cm<sup>-2</sup> for a rate of one count/s. A photon-index power-law of 1.7 and a mean  $N_H$  value of  $2.6 \cdot 10^{20}$  cm<sup>-2</sup> are assumed. The two MOS cameras are assumed to be identical.

Detector	B band	CD band
MOS	5.0	23
pn	1.5	7.9

tended sources classified in the customary C1 and C2 classes (see Section 3.6) plus all point-like sources with a point source detection likelihood ( $LH$ ) greater than 15 (so-called *non-spurious*). The resulting sky coverage is shown in Fig. 2.

### 3.1.1 Count rate and Flux

As in Paper I, fluxes are not computed by XAMIN but are inserted in the catalogue as *derived parameters*, i.e. a single mean flux ( $[\text{FLUX}(\text{MOS}) + \text{FLUX}(\text{pn})]/2$ ) is computed from the count rates using the customary conversion factors reported in Table 3, assuming the spectral model given in its caption.

The observed logN-logS distributions are presented in Fig. 3 reproduced in a simplified form from Elyiv et al. (2012).

Photometric accuracy plots based on simulations were presented in Fig. 3 of Paper I as a function of different off-axis angle ranges. Further simulations were performed considering different background levels as an additional parameter and are presented, supplementing Paper I, in Fig. 4 (the "background factor" of 0.25, 1 and 4 refer to the nominal particle background defined in Table 1 of Elyiv et al. (2012); the latter paper, to which we refer for details, gives also an alternate view in its Figs. 11 and 12). We conclude that the extremely weak dependency on background (if any) does not require to introduce it into the parametrization of photometric bias and accuracy as a function of count rate and off-axis angle published in Table 6 of Paper I.

## 3.2 Positional accuracy and astrometric corrections

The XAMIN pipeline does not provide directly error values, since, for efficiency purposes, the likelihood surface is only searched for its maximum. Therefore, identically to what was done in Paper I, the positional (*statistical*) error on the (point-source) coordinates is estimated from Monte-Carlo simulations, and the values indicated in the catalogue are computed from a look-up table of discrete values as a function of count rate and off-axis angle ranges (as reported in Table 4). The distribution of the errors is shown in panel (b) of Fig. 5.

Similarly to Paper I, in order to compensate for possible *systematic* inaccuracies in the *XMM* pointing positions, a global rigid astrometric correction was estimated using the SAS task EPOSCORR (with rotational offset search disabled). The correction offsets were computed afresh for the full exposure case, and applied to both the 2XLSSd and 2XLSS catalogues.

The input to EPOSCORR were, for each pointing, an X-ray reference file with all *non-spurious* X-ray sources, while optical reference files were generated taking all objects in the CFHTLS W1 fields within 6'' from the (raw) source position, brighter than  $i' = 25$  (or  $r' = 25$  for the ABC fields, see Section 4.1), and having a chance probability (as defined in Section 4.3)  $prob < 0.03$ . In

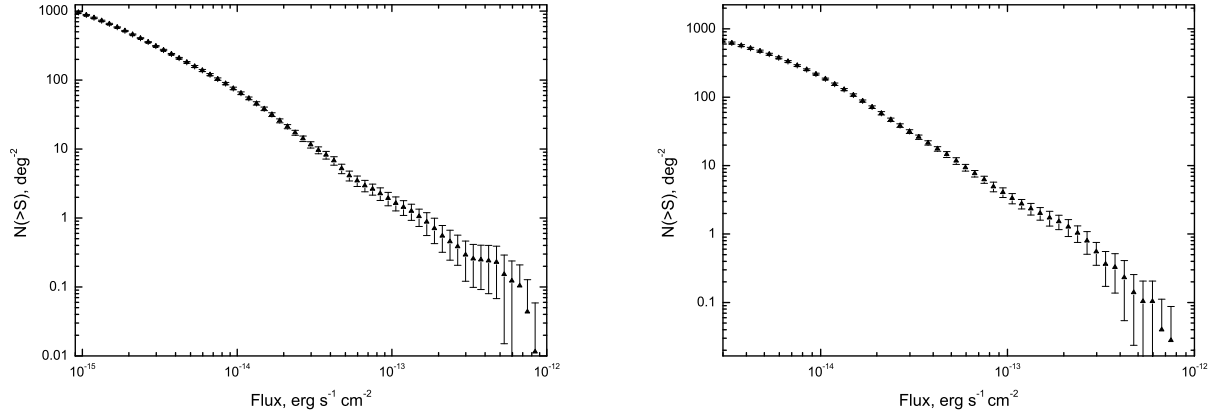


**Figure 3.** The logN-logS distributions for the soft (left-hand panel) and hard (right-hand panel) for the entire *XMM*-LSS area. These figures are reproduced in a simplified form from Figs. 13 and 14 of Elyiv et al. (2012)

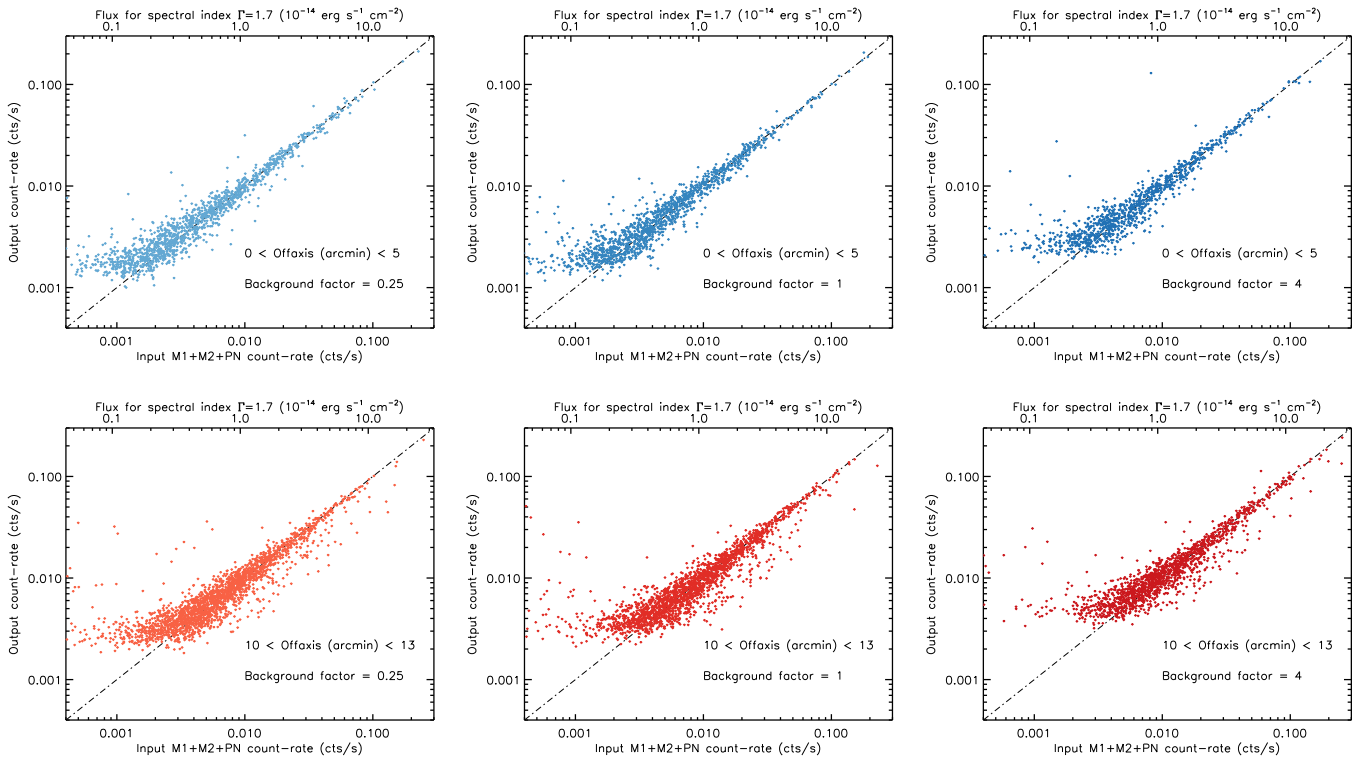


**Figure 4.** Photometric accuracy for three background values (see text) and two off-axis angle ranges (top:  $0-5'$  and bottom:  $10-13'$ ; plots for the intermediate range are rather similar). “Count-rate” is the measured MOS1+MOS2+pn rate, normalised to the on-axis value.

case of more possible counterparts, the one with the smallest probability was taken. Fields B68a and B68b (both bad) had no CFHT counterparts and were corrected using stars in USNO A2.0. Field G12a (bad) had no counterparts at all and was not corrected.

The offsets computed by EPOSCORR were applied to all coordinate sets for each source in the database. Astrometrically corrected positions were used in the subsequent operations: removal of the redundant sources, source naming and cross-identification with the catalogues in other wavebands.

In most cases the offsets are rather small and barely significant<sup>8</sup> The range of the RA offset is  $-3.7'' < \Delta RA < 1.1''$  (with just 16 pointings with  $|\Delta RA| > 2''$ , 27 pointings with a significance of the offset greater than  $3\sigma$ , of which 13 above  $4\sigma$ ). The range of the Declination offset is  $-2.7'' < \Delta Dec < 2.7''$  (with

<sup>8</sup> tabulated online at <http://cosmos.iasf-milano.inaf.it/~lssadmin/Website/LSS/List/newastroreport.html>

**Table 4.** Positional accuracy ( $1\sigma$  error on R.A. or Dec.) for point sources derived from simulations of 10 ks pointings and having a detection likelihood  $> 15$ . Values are given for the B and CD bands, as a function of the summed measured count-rate:  $CR = \text{MOS1} + \text{MOS2} + \text{pn}$ . This table is reproduced from Table 8 of Paper I, to which the reader is referred for further details.

Band	B	CD
Count rate (count/s)	Error (")	Error (")
<hr/>		
$0 < \text{off-axis} < 5'$		
$0.001 < CR < 0.002$	2.0	2.0
$0.002 < CR < 0.005$	1.7	1.7
$0.005 < CR < 0.01$	1.3	1.3
$CR > 0.01$	0.8	0.8
<hr/>		
$5' < \text{off-axis} < 10'$		
$0.001 < CR < 0.002$	2.0	2.0
$0.002 < CR < 0.005$	1.8	1.9
$0.005 < CR < 0.01$	1.5	1.5
$CR > 0.01$	1.0	1.0
<hr/>		
$10' < \text{off-axis} < 13'$		
$0.001 < CR < 0.002$	-	-
$0.002 < CR < 0.005$	1.9	2.0
$0.005 < CR < 0.01$	1.6	1.7
$CR > 0.01$	1.2	1.3

just 4 pointings with  $|\Delta Dec| > 2''$ , 7 pointings with a significance greater than  $3\sigma$ , of which 3 above  $4\sigma$ ).

The quality of the positional accuracy can be estimated *a posteriori* from figures like Figs. 5 and 8. For a final statistics see Section 5.2.

### 3.3 Band merging

The XAMIN pipeline has been optimized for the detection of clusters (which occurs preferentially in the soft band), and its wavelet filtering component is inherently working on a single band (see Pacaud et al. (2006) and references therein), therefore it is natural that energy bands are treated separately and the merging is performed at the post-processing stage, namely in the database ingestion stage. Since, as in Paper I, we intend to provide an X-ray band-merged catalogue along with the single-band ones, such a merging procedure was defined in Paper I to cope with the case that an X-ray source can be detected in one or two bands and, for each band, can be independently fitted by the extended and point source models with the coordinates free. For each band, a source is classified as extended (E) as described in Section 3.6, otherwise it is classified as point-like (P). Then, pointing by pointing, we flag associations between the 2 bands within a search radius of  $10''$ . Note that we allow associations involving spurious sources ( $LH < 15$ ) at most in one band. We keep the information (rate, flux, etc.) about entries below this threshold in the merged catalogue, since it could be more useful (e.g. for upper limits) than no information at all, but we flag those cases with  $B_{\text{spurious}} = 1$  or  $CD_{\text{spurious}} = 1$ . Finally, for each soft-hard couple in the merged catalogue, we define the *best band*, i.e. the band in which the detection likelihood of the source is the highest and from which the coordinates are taken. The source flagging and classification (and the way fluxes appear in the database) is identical to the one described in Tab. 9 of Paper I.

*The change with respect to Paper I is the increase of the search radius from 6 to 10''. In fact an examination of the XLSS catalogue showed an excess of couples of soft-only and hard-only sources*

**Table 5.** Statistics of the band merging procedure

Number of sources for condition	total	non-spurious
in input soft-band table	10348	7339
in input hard-band table	7124	3235
after initial merging	14216	
of which preserved w.r.t. $6''$ merging	13713	7824
of which upgraded	505	457
lost (no longer considered)	492	
$X_{\text{maxdist}} < 2''$	33%	37%
$X_{\text{maxdist}} < 4''$	69%	75%
<hr/>		
after “divorce” procedure		
preserved	13724	
upgraded	492	

usually detected in the same pointing with a distance marginally above  $6''$ . They could be interpreted as “potential missed mergers” since they might have escaped band-merging because of the distance. Or, if they were in different pointings, they could be “potential missed overlaps”. We performed a thorough analysis of sources closer than  $30''$ . 95% of the detections in the same field before band merging, closer than  $10''$ , meet the definition of missed mergers, while only 25% of those farther than  $10''$  do.

The *starting point* is represented by the individual band tables. After the initial merging procedure for 2XLSSd one can directly compare the  $10''$  and  $6''$  merging as shown in Table 5, where (a) “preserved” means they are either unmerged (single band detection) or merged in the same way, and identical in all respects; (b) “upgraded” means they would have been considered at  $6''$  as detections in a single band, and are merged into one at  $10''$ ; (c) lost means single-band detections at  $6''$  no longer considered.

As already described in Paper I, there is a limited number of cases where the band merging is *primarily* ambiguous, and a source in a band happens to be associated with two different objects in the other band (i.e. gives rise to a couple of entries in the merged table). The implication on source naming is discussed below in Section 3.5. In a further step of the band merging procedure we also considered *secondary* ambiguous cases based on the inter-band distance (database column  $X_{\text{maxdist}}$ ) between the positions found by XAMIN in the two energy bands: if in a couple both  $X_{\text{maxdist}} < 6''$  (i.e. they would have been ambiguous also with the old merging), or both  $X_{\text{maxdist}} > 6''$  (irremediably ambiguous), both merged entries are maintained; when one  $X_{\text{maxdist}}$  is below  $6''$  and the other above, the latter entry is *divorced*. The lower-distance element remains a merged two-band detection, while the other is reset to an only-hard or only-soft source.

Note that not all sources in the produced merged table will go into the catalogue: those which are spurious in both bands will not go, as well as those removed as redundant according to the procedure in Section 3.4. The total number of ambiguous cases in the final catalogue is really small: 20 couples and 5 singles (over 6721) for 2XLSSd and 15 couples and 8 singles (over 5572) for 2XLSS.

For sources detected in both energy bands, the inter-band distance  $X_{\text{maxdist}}$  is an additional indicator besides the nominal position error described in Section 3.2. Its distribution is reported in panel (a) of Fig. 5. If we compute a statistical position error  $\sigma$  combining quadratically the nominal errors in the two bands, we can also see that for 2XLSSd 38% have  $X_{\text{maxdist}} \leq \sigma$ , 76% within

$2\sigma$  and 93% within  $3\sigma$  (for 2XLSS the percentages are 30%, 67% and 88% respectively).

### 3.4 Removal of redundant sources

As in Paper I, in the case of redundant objects detected in the regions where the pointings overlap, we keep in the catalogue only the detection pertaining to the pointing where the source is the closest to the optical centre (columns `Boffaxis`, `CDoffaxis` in the database). Since overlap removal is the final stage of catalogue building, it is here that sources with  $LH < 15$  are discarded and only non-spurious sources are brought forward. However, at variance with Paper I, for analogy with the band merging, redundant objects are associated within a larger radius of  $10''$ . Moreover, the off-axis angle criterion is applied only if the overlapping pointings are both flagged good or both bad, otherwise the source in the good pointing prevails unconditionally.

The overlap removal affects 1574 entries in 2XLSSd and 1205 in 2XLSS.

Note that the present catalogue also contains a few sources in fields flagged bad. An extremely conservative usage may exclude all sources detected in bad fields using condition `Xbadfield = 0`. A less conservative one should include the 4 (bad, non-reobserved) fields mentioned in the caption of Table 1,

### 3.5 Source naming

Application of the latest XAMIN version, of the updated CHFTLS T004 astrometric corrections, and of the  $10''$  radius in the band merging and overlap removal stages, implies that, even in the pointings already covered by the Version I XLSS catalogue, a source may be sometimes superseded by a different choice, and anyhow may have slightly different coordinates. The same applies to the two processings (full exposures and 10 ks exposures). This, combined with the IAU requirement that once a source in a catalogue has been assigned a name (even if this is a "coordinate name"), the name cannot change even if the actual coordinates are improved (modified), unless a completely new catalogue is issued, lead us to define the following naming convention:

(i) the "official" catalogue name `Xcatname` is now generated in the form `2XLSS Jhhmmss.s-ddmmss`, or respectively `2XLSSd Jhhmmss.s-ddmmss` where, as in Paper I, the coordinates used in assigning the name are the ones deduced after the rigid astrometric correction, and chosen as official, i.e. those for the *best band* (see Table A2).

(ii) the single-band catalogue names `Bcatname` and `CDcatname` use the unofficial prefixes `2XLSSB` or `2XLSSCD` for both the deep and 10 ks catalogues. However, as in Paper I, the coordinates used in the name correspond to the extended (E) or point-like (P) fit in the relevant band (Table A2).

(iii) the reference to the XLSS source replaced by a 2XLSS or 2XLSSd source is possible using column `Xlsspointer` which contains the value of `Xseq` in the table `XLSS` (an explicit look-up in the latter table is necessary to find its name or other characteristics).

(iv) Similarly, when accessing 2XLSS it is possible to use column `Xdeep` which points to the value of the `Xseq` closest source in 2XLSSd.

As described above in Section 3.3, in a small number of cases, a source in a band happens to be associated with two different objects in the other band. These couples of catalogue entries are

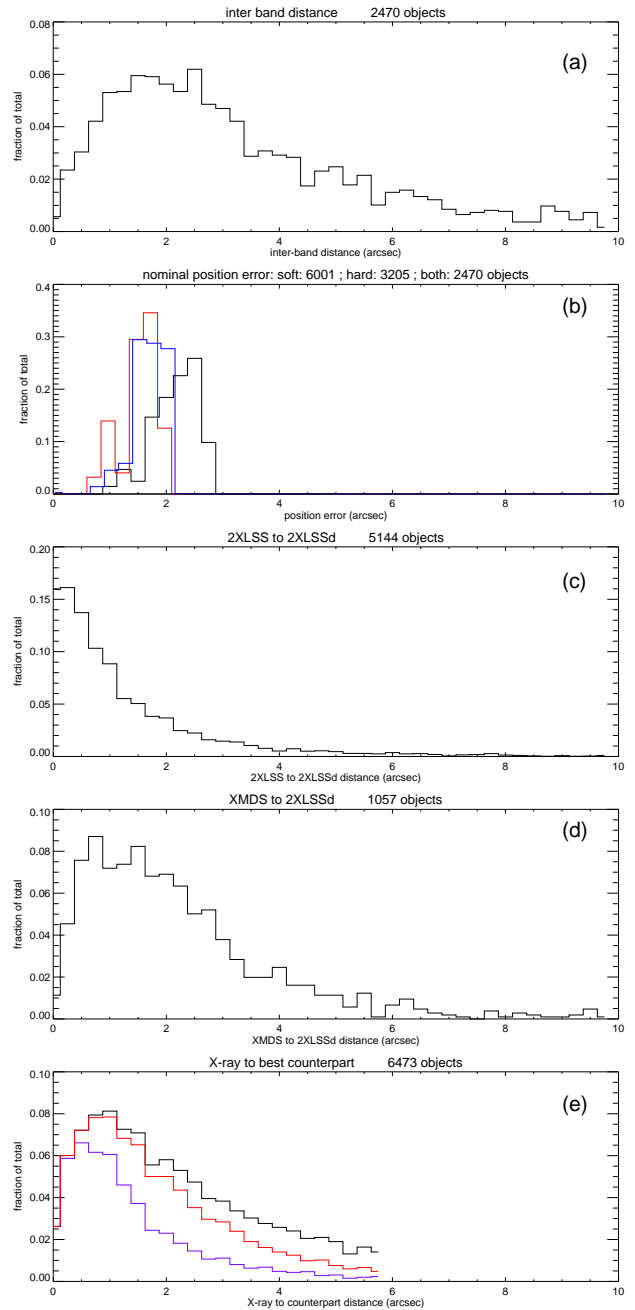


**Figure 5.** Histograms (as a fraction of the total number of objects indicated in each panel title) of distances or positional parameters for the 2XLSSd catalogue. Panel (a) gives the distribution of the inter-band distance `Xmaxdist` for objects detected in both energy bands. Panel (b) gives the distribution of the position errors for the soft (light gray histogram, red in the web version) and hard (light gray histogram, blue in the web version) bands, and of their combined error for sources detected in both bands (black histogram). Panel (c) gives the distance between the X-ray positions in the two catalogues for objects common to 2XLSSd and 2XLSS (both resulting from same XAMIN pipeline). Panel (d) gives the distance between the X-ray positions in the two catalogues for objects common to 2XLSSd and XMDS (different event file reduction and different pipeline, see Appendix C3). Panel (e) gives the distribution of the distance between the X-ray position and the position of the best counterpart in the optical, NIR, IR or UV band. The black histogram is for all the objects with a counterpart (of any quality) in at least one non-X-ray band. Also shown (*as a fraction of the same total*) the distributions for the counterparts having either good or fair probability (light gray histogram, red in the web version), and for those having good probability (gray histogram, violet in the web version).

**Table 6.** Statistics of extended sources

Classification and catalogue	2XLSS	2XLSSd
sources with Bc1c2 $\neq$ 0	147	160
of which C1	49	53
of which C2	98	107
total no. of extended sources	187	210
of which C1	54	57
of which C2	133	153
extended in both bands	4	4
soft C1 detected in both bands	9	12
soft C2 detected in both bands	12	16
soft only C1	36	37
soft only C2	86	91
hard only C1	5	4
hard only C2	35	46

flagged by a non-zero value in column `Xlink`, Consistently with the convention defined in Paper I, the ambiguity in the name is resolved (when necessary, i.e. in 1 case for 2XLSSd and 3 cases in 2XLSS) by the addition of a suffix: e.g. the two members of a couple will appear as 2XLSS JHHMSS.S-DDMMSSa and 2XLSS JHHMSS.S-DDMMSSb.

### 3.6 Extended source classification

The extended source classification is the same as described in Paper I. Extended sources are selected from the XAMIN parameter space as detections with `extent`  $> 5''$ , `likelihood of extent`  $> 15$ , and further divided into two classes: C1 with `likelihood of extent`  $> 33$  and `likelihood of detection`  $> 32$ , which is almost uncontaminated by misclassified point sources, and C2 (the rest), allowing for  $\approx 50\%$  contamination. This classification is rather stable even in case of changes in the exposure time or background, as shown in Fig. 9 of Clerc et al. (2012a)

The catalogues report only the flagging as extended source in the soft band (column Bc1c2). However, for the unique purpose of band merging, the same classification has nominally been applied also to the hard band. A short statistics is reported in Table 6, while the compatibility in the two catalogues (*compatible* means extended in both catalogues in the (prevailing) band where it is detected, and undetected (or point-like) in the other band) is shown by this breakdown:

- 95 sources with same extended classification
- 8 sources with compatible classification
- 1 soft extended in 2XLSS, hard extended in 2XLSSd
- 23 point-like in 2XLSS, extended in 2XLSSd
- 20 extended in 2XLSS, point-like in 2XLSSd

Studies of galaxy clusters in the XMM-LSS are presented in Adami et al. (2011), Willis et al. (2012) and Clerc et al. (2012b). More information on confirmed clusters is also available in the XMM-LSS survey cluster database<sup>9</sup>.

<sup>9</sup> <http://xmm-lss.in2p3.fr:8080/l3sdb/>

## 4 GENERATION OF THE MULTIWAVELENGTH CATALOGUE

### 4.1 The input catalogues

Most of the XMM-LSS area was covered in the  $u^*, g', r', i', z'$  bands by the W1 Wide Synoptic field of the CFHTLS, and the core area (our G pointings in Table 1, corresponding to the XMD5) also by the 1 deg<sup>2</sup> Deep field D1. The northernmost strip  $\delta \gtrsim -3.7^\circ$  was not part of CFHTLS and was observed under a Guest Observer program in a similar configuration at the CFHT (but only in the  $g', r', z'$  bands) with three pointings (so called ABC fields), leaving a gap only in correspondence of the bright star Mira Ceti.

We used a compilation of the Terapix<sup>10</sup> panchromatic catalogues for W1 (release T004) and the ABC fields, edited to get rid of duplicates in overlapping pointings, and replacing undefined magnitudes due to non-detection in one band with the limiting magnitude of the pointing. Separately we also used the panchromatic catalogue of the D1 field.

Most of the XMM-LSS area was also observed by the *Spitzer Space Telescope*, as part of the SWIRE survey (Lonsdale et al. 2003). We obtained from IPAC a compilation of an unpublished release catalogue in the 4 IRAC (3.6, 4.5, 5.8 and 8.0  $\mu\text{m}$ ) and 3 MIPS (24, 70 and 160  $\mu\text{m}$ ) bands, which was pre-processed for classification of extended objects; in particular IRAC fluxes are Kron fluxes for extended objects and so-called aperture 2 (1.9'') otherwise, while they are APEX (PRF) fluxes for MIPS.

For the UKIDSS NIR survey we retrieved from the WSA public archive<sup>11</sup> data (within 10'' from our X-ray source positions) from the release DR5plus, which at the time provided partial coverage of some areas of the XMM-LSS via the DXS and UDS surveys (in particular the latter covers the SXDS area).

For the UV band we retrieved from the NASA MAST public GALEX archive<sup>12</sup> (using the CASJOBS tool) data from the GR4/GR5 release (within 10'' from our X-ray source positions). Since it is well known that the MAST GALEX catalogue contains redundant sources where GALEX pointings overlap (so called *tiling artifacts*), we have run a procedure to flag GALEX objects within 1.5'' from any other one observed in a different tile, and to prefer in each set the one observed in two bands, or with smallest inter-band separation, or with smallest off-axis angle.

The coverage of the XMM-LSS area by the various catalogues is shown in Fig. 1.

All appropriate data were ingested in tables within our database and elaborated therein with the procedure described below (the optical data were also used separately for the *preventive* astrometric correction described in Section 3.2).

### 4.2 The candidate definition procedure

As a preliminary step, we construct within our database correlation tables between the X-ray sources in either 2XLSS or 2XLSSd and *each one independently* of the CFHTLS D1, W1, SWIRE, UKIDSS and GALEX tables, using a radius of 6''.

The next step is an *incremental addition* procedure through the above tables in the quoted order:

- (i) We create a generalized correlation table, with columns designated to hold pointers to the various catalogues, initialized

<sup>10</sup> <http://terapix.iap.fr/>

<sup>11</sup> <http://surveys.roe.ac.uk/wsa/>

<sup>12</sup> <http://galex.stsci.edu/GR4/>

with as many records as X-ray sources. Each record is an n-uple  $(X, D1, W1, SWIRE, UKIDSS, GALEX)$  initialized as  $(X, 0, 0, 0, 0, 0)$ . Records are termed *counterpart sets*.

(ii) We start with the D1 table and for each X-ray source we *insert a pointer* in the relevant record if there is at least one D1 object within  $6''$ . If the X-ray source has one optical counterpart only, the D1 pointer is *inserted* in the existing primary record, so the n-uple is filled as  $(x_1, d_a, 0, 0, 0, 0)$ .

If it has more, the pointer of the closest candidate is inserted as above, while *additional records are added* copying from the primary one and replacing the pointer with one associated with the other D1 object, e.g. an additional n-uple  $(x_1, d_b, 0, 0, 0, 0)$ .

(iii) Then one proceeds in turn to the next table *inserting* an object from such a table when it is closer to one of the existing counterparts in other non-X-ray tables within a predefined radius. Only objects within  $6''$  from the relevant X-ray source are considered, while a correlation radius of  $0.5''$  is used when comparing positions of the same origin (i.e. D1 and W1), of  $1''$  when comparing to SWIRE or UKIDSS catalogues, and of  $1.5''$  when comparing to GALEX.

(iv) A pointer is *inserted* in an existing record when there is a single match with the X-ray position and all the positions in the previously processed catalogues. E.g. an n-uple is updated as  $(x_1, d_a, w_a, 0, 0, 0)$ . *Additional counterpart sets are generated* in all other cases (typically an independent counterpart of the X-ray source with no counterpart in previous catalogues, but could also be an ambiguous association of more sources in the current catalogue with a previously defined counterpart set). E.g. in the case of W1 objects they are compared with D1, while SWIRE objects are compared first with W1, then D1; UKIDSS objects are compared with preceding tables (in order W1, D1, SWIRE); and GALEX objects are compared with all other tables (in order W1, D1, SWIRE, UKIDSS). One may therefore end up with completely or partially filled pre-existing n-uples like  $(x_1, d_a, w_a, s_a, 0, g_a)$ , or with new n-uples like  $(x_1, 0, w_n, s_n, u_n, 0)$  or  $(x_1, 0, 0, s_p, 0, 0)$ , or (seldom) with ambiguous cases like  $(x_1, d_b, w_b, 0, 0, g_q)$  and  $(x_1, d_b, w_b, 0, 0, g_r)$ .

(v) Finally the chance probabilities for random association of a counterpart with the X-ray source are computed as described immediately hereafter.

### 4.3 Computing probabilities and counterpart ranking

We compute *four* probabilities:  $\text{probX0}$ ,  $\text{probXS}$ ,  $\text{probXU}$  and  $\text{probXG}$ ; each is the probability of chance coincidence between the X-ray source and its counterpart in a given catalogue, based on the X-ray to optical (or SWIRE, UKIDSS or GALEX) distance, the optical, IR or UV intensity (magnitude or flux)  $m$ , and the density of sources brighter than such an intensity. They are based on a formula (Downes et al. 1986) like

$$\text{prob} = 1 - \exp(-\pi n(\text{brighter than } m) r^2) \quad (1)$$

where  $r$  is the X-ray to counterpart distance, while a rough estimate of the density  $n(\text{brighter than } m)$  is computed as described in detail in Appendix B.

At this stage each X-ray source can have more than one potential counterpart (or better, counterpart sets, where each set may include associated counterparts in D1, W1, SWIRE, UKIDSS and GALEX). A preliminary ranking can be assigned on coarse probability ranges:

good if  $\text{prob} < 0.01$

fair if  $0.01 < \text{prob} < 0.03$

bad if  $\text{prob} > 0.03$

The acceptable tuning with the data of such coarse classification is demonstrated by Fig. B1. Such a pre-ranking is refined by a multi-step heuristic procedure, which assigns a score based on several criteria (for instance weighing more a good or fair probability in the optical or SWIRE bands, or the fact that the best probability of a counterpart set is at least 10 times better (smaller) than those of any other counterpart set for the same X-ray source, or whether the counterpart set is unique, or brightest and closest). In some cases a visual inspection of the optical thumbnail (see Section 2.4.2.2) with the overlay of all counterpart set elements has been necessary. In exceptional cases this resulted in a manual editing (usually deletion of counterpart sets due to artifacts, like unresolved tiling effects in one of the catalogues, or problems near very bright or saturated sources).

The result of the ranking is the assignment of the value of column  $\text{Xrank}$  (see Table A3) in the multiwavelength catalogues  $2\text{XLSSOPT}$  or  $2\text{XLSSOPTd}$  (derived respectively from the 10 ks and deep X-ray catalogues).

The number of *potential* counterpart sets can be rather high (16813 for  $2\text{XLSSOPT}$  and 20837 for  $2\text{XLSSOPTd}$ ). However a large number of them (9093 and 11500), based on the above ranking procedure, obtain a rank  $\text{Xrank} = -1$ , which means they have to be rejected. This leaves 7720 or resp. 9337 potential counterpart sets in the publicly released  $2\text{XLSSOPT}$  or  $2\text{XLSSOPTd}$ . Such non-rejected counterpart sets, as the result of an ambiguity analysis, have  $\text{Xrank}$  between 0 and 2. For X-ray sources with a single counterpart set (either physically unique or just one non-rejected)  $\text{Xrank}$  is either 0 or 1. When instead an X-ray source has more possible counterpart sets, there is a single one which has  $\text{Xrank} = 0$  or  $\text{Xrank} = 1$ , i.e. the preferred, while all the secondaries have  $\text{Xrank} = 2$ . More details on ranks, together with a detailed statistics, are presented in Section 5.2.1. The rank, and the potential counterpart list, are provided as a convenience for database users, but are not at all intended as prescriptive. Additional information about visual, spectroscopic and SED classification of X-ray sources with respect to the optical counterparts may be found in Melnyk et al. (2012).

## 5 A FEW STATISTICS

### 5.1 The X-ray catalogues

The number of sources in the merged 10ks catalogue is 5572 for  $2\text{XLSS}$  (4932 in  $2\text{XLSSB}$  and 1923 in  $2\text{XLSSCD}$ ). The number of sources in the deep catalogue is 6721 for  $2\text{XLSSd}$  (5881 in  $2\text{XLSSBd}$  and 2645 in  $2\text{XLSSCDd}$ ).

A majority of objects detected in the full exposures are confirmed in the 10 ks exposures, usually with the same classification and within a distance of  $6''$ ; the differences are concentrated within the objects with poorer likelihood. However there is a significant number of detections, not necessarily spurious, which are either present only in the full exposures (not surprising) or even only in the 10ks exposures. If one considers data *before* band merging *and* spurious source filtering, 24% of the soft detections and 40% of the hard detections in full exposures are not confirmed in 10 ks ones, while 8% (soft) and 19% (hard) 10 ks detections are new.

Considering band merged data *before* overlap removal (and spurious source filtering), 29% of the merged detections in full exposures are not confirmed in 10 ks ones (mainly single soft non-

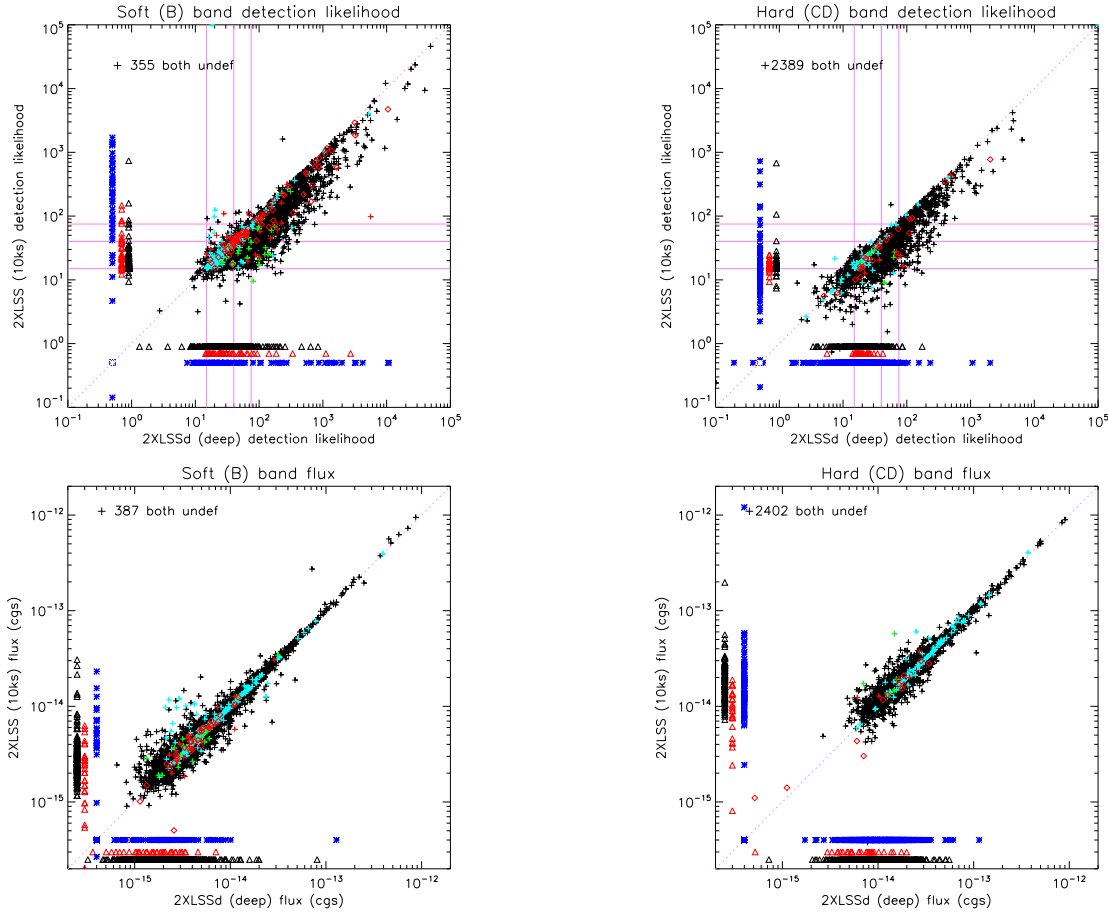


**Figure 6.** Comparison of the detection likelihood (top row) and of the flux (bottom row) in the soft (left column) and hard (right column) energy bands between 2XLSS and 2XLSSd. Crosses and diamonds indicate point-like or extended objects associated in the two catalogues (see text). Blue asterisks indicate likelihood or flux are present but *undefined* in one catalogue, while triangles indicate sources present only in one catalogue (both are placed at a conventional out-of-range X or Y position). The number of objects with undefined values in *both* catalogues in a given band, but nevertheless associated, is indicated near the top left corner of each panel. Colour coding (only in the web version) is as follows: black cross for point-like common sources in 2XLSS good fields; cyan cross idem for bad fields; green cross for 2XLSSd extended object point-like in 2XLSS; vice versa for red cross; red diamond for extended sources in both 2XLSS and 2XLSSd. Triangles are black or red for point-like or extended sources which are either new in 2XLSS or present in 2XLSSd but lost in the shallower catalogue. In the likelihood plots, the thin pink lines are fiducial marks corresponding to the spurious/non-spurious threshold (15) and to the conventional  $3\sigma$  (40) and  $4\sigma$  (75) levels.

**Table 7.** Basic statistics for the 2XLSS and 2XLSSd catalogues

Case	2XLSSd	2XLSS
Total number of sources	6721	5572
Detected in both bands		
non-spurious in both bands	27%	23%
non-spurious in soft band only	8%	8%
non-spurious in hard band only	2%	1%
Detected only in soft band	52%	57%
Detected only in hard band	11%	10%
Not detected in other catalogue	24%	9%

spurious, or in similar proportion between hard and soft when spurious), while 14% of the 10 ks detections are new (the majority are spurious, but mainly single detections in the soft band prevail when non-spurious).

We proceed below to some further comparison between the deep and 10 ks catalogues, which allows us to assess a trade-off

between deeper but disuniform exposures and shallower uniform exposures. A comparison with the Version I (XLSS) release is reported in Appendix C1.

While sources in a *catalogue* are by construction non-spurious (i.e. with  $LH > 15$  in at least one band), they can be detected as such in both bands, detected as non-spurious in one band and spurious in the other, or detected in a single band. The breakdown in percentage is reported in Table 7. The deep catalogue is marginally better for what concerns full-fledged both band detections.

A breakdown considering also the classification for the 5117 common objects can be summarized as follows: 85% are classified point-like identically in both catalogues (which means either point-like or undetected in each band), which goes up to 97% classified point-like and compatible (i.e. detected in both bands in one catalogue and in a single one in the other); 2% are classified as extended (usually identically, only compatible in 8 cases, while in 1 single case the source is detected as extended once in the soft and once in the hard band); the few remaining cases are 23 2XLSSd and

20 2XLSS extended sources which are point-like in the other catalogue.

The distances between common objects are in very good agreement: 90% within  $2''$ , 97% within  $4''$ , and 99% within  $6''$  (see also panel (c) of Fig. 5).

A comparison of likelihoods and fluxes for sources associated is reported in Fig. 6. As expected the likelihood in the shorter exposure 2XLSS catalogue is compatible but lower than the one in 2XLSS<sub>d</sub> (the points lay below the diagonal fiducial line of equal values).

For fluxes they are generally rather well consistent (with exceptions for a few extended sources), with only a moderate scatter for fainter objects. In lack of error bars, one can compare the compatibility of fluxes for the 5144 sources associated between 2XLSS<sub>d</sub> and 2XLSS. For the 4656 with a soft-band detection in both catalogues, 60%, 81% and 96% of the sources have fluxes within 10%, 20% or 50%. The equivalent percentages for the 2146 with a hard-band detection are 53%, 77% and 95%.

In Fig. 7 we provide also an histogram of the fluxes, mainly for the 2XLSS catalogue (but the shaded area indicates what we "gain" at low fluxes passing from 10 ks to full exposures).

## 5.2 The multiwavelength catalogues

### 5.2.1 Statistics on each catalogue

We first present some general statistics on both catalogues in parallel, quoting values for 2XLSSOPT, followed by those for 2XLSSOPT<sub>d</sub> in parentheses.

To evaluate whether in a given region we do not find counterparts in a given wavelength table because they do not exist or because the region has not been observed at all, one should refer to Fig. 1.

2XLSSOPT (2XLSSOPT<sub>d</sub>) starts from 16813 (20837) nominal counterpart sets, from which we removed the 9093 (11500) rejected ( $X_{\text{rank}} = -1$  as explained in Section 4.3).

X-ray sources nominally flagged as *blank fields* (i.e. having a single *null counterpart set*, i.e. no catalogued CFHTLS, SWIRE, UKIDSS or GALEX counterpart within  $6''$ ) are 221 (248). Note that the absence of catalogued sources does not mean they are necessarily real blank fields. Often bright sources are omitted by the catalogues, but are visible if one inspects the thumbnail image. Compare for instance the cases of sources 2XLSSOPT.Xseq = 43302, which is very close to a  $R=15.6$  galaxy shown in SIMBAD, or 2XLSSOPT.Xseq = 38678 whose field is spoiled by the nearby bright star BD-05 427. So some of the cases flagged as blank field can instead have a bright counterpart.

Concerning tentative identifications of 5572 (6721) X-ray sources:

- 18% (17%) have a *physically single counterpart (set)*
- 40% (39%) have a *single very reliable counterpart*, i.e.  $X_{\text{rank}} = 0$  plus eventual *rejected* counterpart sets
- 21% (28%) have a *single, but not so reliable, counterpart*, i.e.  $X_{\text{rank}} = 1$ , also plus eventual *rejected* counterpart sets
- 16% (16%) are *pseudo-ambiguous*, with one *definitely preferred* counterpart ( $X_{\text{rank}} = 0$ ), plus one or more nominal secondary counterparts with rank 2.
- 13% (14%) are *definitely ambiguous*, with one *nominally preferred* counterpart ( $X_{\text{rank}} = 1$ ), plus one or more secondary coun-

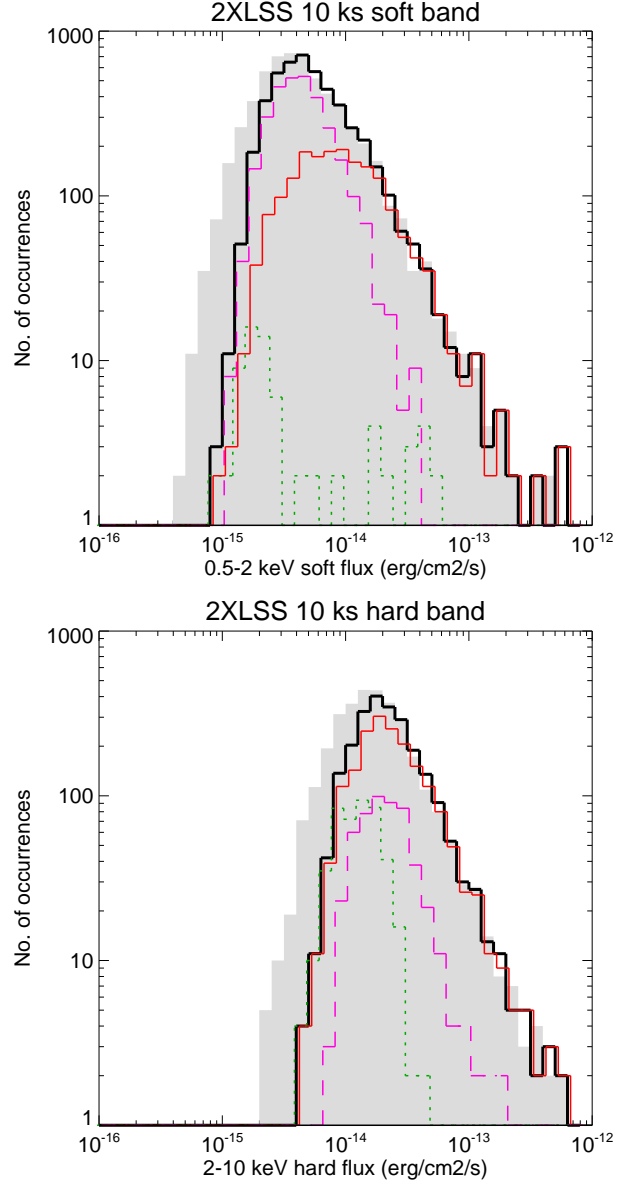


**Figure 7.** Histogram of the soft (top panel) and hard (bottom panel) fluxes. The gray shaded histogram in the background refers to the 2XLSS<sub>d</sub> deep catalogue. All other histograms refer to the 2XLSS 10 ks catalogue, and namely to: all sources in the band (thick black); sources detected in both bands (thin solid red); sources detected only in the band (hence by definition non-spurious; thin dashed magenta); fluxes with a spurious likelihood in the band, associated with a non-spurious source in the *other* band (thin dotted green). Colours are shown only in the web version. The various histograms are slightly offset for clarity.

terparts with rank 2, at least one of which is not terribly worse than the nominally preferred one.

With reference to the criteria defined in Section 4.3, 48.2% (48.6%) of the sources have a best counterpart with a good probability, 29.5% (30.1%) with a fair one, and 4.0% (3.7%) are nominal blank fields.

One might also relate the counterpart association with the X-ray detection significance (using the cross calibration between likelihood and number of  $\sigma$  presented in Appendix C3.1): for instance of 1412 (1888) X-ray sources detected above  $4\sigma$ , 77% (76%) have

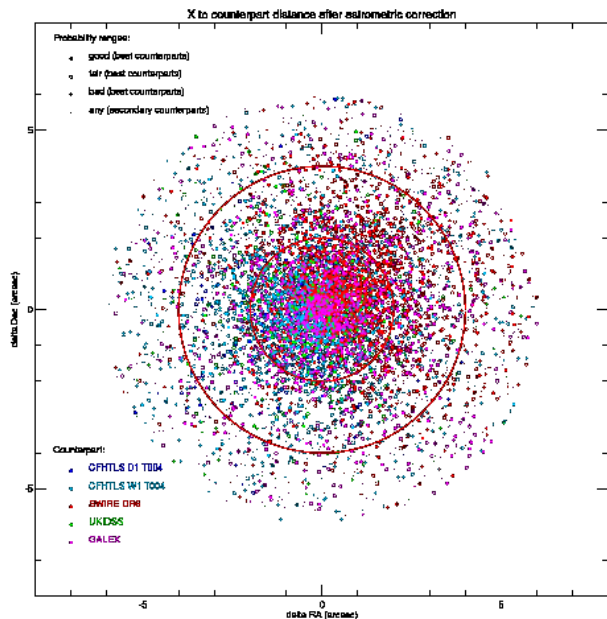


**Figure 8.** Distances in RA and Dec between the X-ray corrected position and the counterpart position. Different symbols indicate the identification quality. A circle is plotted when the counterpart is the best one, and the chance probability is good or fair (filled in case of good probability). A cross is plotted for the best counterpart when the probability is bad. A dot is plotted for secondary (ambiguous) counterparts, irrespective of probability, but only if it is good or fair. Different colours (web version only) or shades (as shown on figure) indicate the origin of the counterpart position for the distance calculation. Two fiducial radii of 2 and 4'' are also shown. This figure refers to 2XLSS; the equivalent figure for 2XLSSd is extremely similar.

a good counterpart, 18% (20%) a fair one, and only 2% (1%) are unidentified; of 2436 (3169) X-ray sources above  $3\sigma$ , 68% (65%) have a good counterpart, 25% (27%) a fair one, and 2% (2%) are unidentified.

One shall also note that the *ranking depends* on the probabilities, and these depend on the distance (Section 4.3) and therefore *ultimately on the X-ray position*. If the latter changes, the rank choice will change. The differences between the two catalogue variants are discussed in the next section.

Finally, the quality of the tentative identifications can be assessed from the offset (distance) between the X-ray source position and the position of the best counterpart in the best counterpart set. This is shown in Fig. 8 and in panel (e) of Fig. 5. 83% (84%) of all counterparts have a distance within 4'', which occurs for 90% (91%) of the best counterparts with fair or good probabilities (the circles in Fig. 8) and for 95% (95%) of those with good probabilities (the filled circles in Fig. 8).

There is some evidence from Fig. 8 of a systematic in the deviations between X-ray positions and positions in the various catalogues. The average deviation for the optical and UKIDSS catalogues clusters around a point in the third quadrant (e.g.  $-0.39''$ ,  $-0.07''$  for W1), while the one for SWIRE clusters around a point in the first quadrant ( $0.82''$ ,  $0.57''$ ). For 2XLSSd ( $-0.40''$ ,  $-0.07''$ ) and ( $0.79''$ ,  $0.52''$ ) respectively.

Concerning panel (e) of Fig. 5, it reports the distribution of the X-ray to counterpart distance, using as counterpart position the one with the smallest distance (in 37% this is an optical source, in 34% a SWIRE one, in 9% a UKIDSS one and in 20% a GALEX one).

### 5.2.2 Differences between 2XLSSOPT and 2XLSSOPTd

The differences between the two catalogues with optical identifications derive from three main reasons, the former two physiological, due to the different exposures:

- (i) the X-ray source may be detected in one of the input catalogues and not in the other
- (ii) the X-ray source may be detected or classified differently (spurious or non-spurious, in one or two bands, point-like or extended)
- (iii) the X-ray source can be detected at a displaced position

The latter displacement may result in some of the possible counterparts be outside the 6'' correlation radius, and therefore in the list of counterpart sets being partially or totally different, and with different ranks.

Considering all potential counterpart sets (including negative rank *rejected* counterparts since rejection may act differently because of the displacement), about 86% of the common ones are identical (i.e. have the same counterparts in all non-X-ray catalogues), of which 139 are confirmed "blank fields" (no *catalogued* counterpart in any waveband). The remaining cases may be altogether different counterpart sets, or partially match (in some of the non-X-ray catalogues). More details are provided in Appendix C2

Concerning the tentative *blank fields* one has to note that, besides the 139 common ones, there are 109 2XLSSOPTd blank fields not present in the 10ks catalogue and 82 2XLSSOPT blank fields which are new in the latter catalogue (42 are new X-ray sources with no deep counterpart, the other 40 are no longer blank fields).

Coming now to *non* blank fields, remember that the identification procedure is incremental. So it starts (in absence of a D1 counterpart) associating a W1 object with the X-ray source. Then it may append one SWIRE object (associated with the X-ray source and within 1'' from W1) to the counterpart set, and create a new counterpart set for another SWIRE object. And so on and so forth for the other wavebands. Each association may be different as a result of a small displacement in the X-ray position. In the most favourable case this may just prefer a particular counterpart in a counterpart set otherwise identical and identically ranked. In other cases counterpart sets similar but differing in one waveband may be ranked differently (primary vs secondary or even rejected).

### 5.3 Comparison with XMDS

This section provides a sketchy comparison between the catalogues presented in this paper and the XMDS (*XMM* Medium Deep Survey) one, a subset of which was published as the XMDS/VVDS  $4\sigma$  catalogue (Chiappetti et al. 2005). Since the entire XMDS catalogue is unpublished, we will release it through our database contextually with Version 2 *XMM-LSS* ones (see Table 2). A comparison provides an opportunity to validate and cross-calibrate two different pipelines (a traditional and an innovative one) on the same input data. The main differences between the two pipelines, and further details of the comparison are reported in Appendix C3.

The XMDS catalogue includes 1168 sources (by definition all in the G-labelled fields) of which 1057 are catalogued in 2XLSSd. Appendix C3.1 provides further details, in particular:

- (i) A cross calibration of the detection likelihood of XAMIN with the significance in terms of the number of  $\sigma$

of the XMDS shows that a likelihood of 75 corresponds more or less to the  $4\sigma$  level, and one of 40 to the  $3\sigma$  level.

(ii) Fluxes match rather well, although with a systematic difference (which, considered the different procedures is fully acceptable), namely  $2XLSSd$  fluxes are 0.895 lower than the XMDS ones in the B band, while they are only 1.040 higher in the CD band.

(iii) Also XMDS fluxes measured *simultaneously* in all bands match well  $2XLSSd$  fluxes measured *separately* for sources detected in both bands, which reinforces trust in the band merging procedure described in Section 3.3.

It is also possible to compare the counterparts in optical (and other) bands between the XMDS and the  $2XLSSOPTd$  catalogue and, as shown in Appendix C3.2, the compatibility between the counterparts is also satisfactory.

#### 5.4 Comparison with 2XMM

We did a quick comparison with the 2XMM (second *XMM*-Newton serendipitous source) catalogue (Watson et al. 2009). Details are reported in Appendix C4. We find, despite the differences in the data processing and in the definition of the energy band, an acceptable match in terms of number of sources, respective distance, and fluxes.

## 6 CONCLUDING REMARKS

We have presented in this paper X-ray full-exposure ( $2XLSSd$ ) and 10 ks-limited exposure ( $2XLSS$ ) catalogues for the  $11.1 \text{ deg}^2$  *XMM*-LSS field. The total number of X-ray sources reported in these two catalogues are 6721 and 5572, respectively. The sources were detected in the 0.5-2 keV and/or 2-10 keV energy bands with a new version (3.2) of the XAMIN pipeline. We have also provided two multi-wavelength catalogues (cross-correlating out the X-ray sources with IR/SWIRE, NIR/UKIDSS, optical/CFHTLS and UV/*GALEX* sources),  $2XLSSOPTd$  and  $2XLSSOPT$ , corresponding to the full and 10 ks-limited exposure catalogues respectively. We have also described in detail the X-ray band merging, the X-ray point-like and extended source classification, the matching procedure of counterparts from multiwavelength surveys as well as extensive statistics to compare the two presented catalogues between them and with previous studies.

Catalogues and associated data products are available through the Milan data base (<http://cosmosdb.iasf-milano.inaf.it/XMM-LSS/>), with a reduced summary stored at CDS.

## ACKNOWLEDGMENTS

The results presented here are based on observations obtained with *XMM-Newton*, an ESA science mission with instruments and contributions directly funded by ESA Member States and NASA. We acknowledge the work done by Krys Libbrecht on the XAMIN pipeline translation.

Optical photometry data were obtained with MegaPrime/MegaCam, a joint project of CFHT and CEA/DAPNIA, at the Canada-France-Hawaii Telescope (CFHT) which is operated by the National Research Council (NRC) of Canada, the Institut National des Sciences de l'Univers of the Centre National de la Recherche Scientifique (CNRS) of France, and the University of Hawaii. This work is based in part on data

products produced at TERAPIX and the Canadian Astronomy Data Centre (CADC) as part of the Canada-France-Hawaii Telescope Legacy Survey, a collaborative project of NRC and CNRS. We acknowledge the help of J.J. Kavelaars of the CADC Helpdesk about thumbnail cutout for the ABC fields.

This work is in part based on observations made with the *Spitzer Space Telescope*, which is operated by the Jet Propulsion Laboratory, California Institute of Technology under NASA. Support for this work, part of the *Spitzer Space Telescope* Legacy Science Program, was provided by NASA through an award issued by the Jet Propulsion Laboratory, California Institute of Technology under NASA contract 1407.

This work is in part based on data collected within the UKIDSS survey. The UKIDSS project uses the UKIRT Wide Field Camera funded by the UK Particle Physics and Astronomy Research Council (PPARC). Financial resources for WFCAM Science Archive development were provided by the UK Science and Technology Facilities Council (STFC; formerly by PPARC).

*GALEX* is a NASA mission managed by the Jet Propulsion Laboratory. *GALEX* data used in this paper were obtained from the Multimission Archive at the Space Telescope Science Institute (MAST). STScI is operated by the Association of Universities for Research in Astronomy, Inc., under NASA contract NAS5-26555. Support for MAST for non-HST data is provided by the NASA Office of Space Science via grant NNX09AF08G and by other grants and contracts.

OM, AE and JS acknowledge support from the ESA PRODEX Programmes "XMM-LSS" and "XXL", and from the Belgian Federal Science Policy Office. They also acknowledge support from the Communauté française de Belgique - Actions de recherche concertées - Académie universitaire Wallonie-Europe".

## REFERENCES

- Adami C., et al., 2011, *A&A*, 526, A18
- Baldi A., Molendi S., Comastri A., Fiore F., Matt G., Vignali C., 2002, *ApJ*, 564, 190
- Bertin E., Arnouts S., 1996,
- Chiappetti L., et al., 2005, *A&A*, 439, 413
- Clerc N., Sadibekova T., Pierre M., Pacaud F., Le Fèvre J.-P., Adami C., Altieri B., Valtchanov I., 2012a, *MNRAS*, 423, 3561
- Clerc, N., et al., 2012b, in preparation
- Downes A. J. B., Peacock J. A., Savage A., Carrie D. R., 1986, *MNRAS*, 218, 31
- Elyiv A., et al., 2012, *A&A*, 537, A131
- Lawrence A., et al., 2007, *MNRAS*, 379, 1599
- Lonsdale C. J., et al., 2003, *PASP*, 115, 897
- Martin D. C., et al., 2005, *ApJ*, 619, L1
- Melnyk, O., et al., 2012, submitted to *A&A*
- Paiero L., Chiappetti L., Garilli B., Franzetti P., Fumana M., Scodreggio M., 2008, *ASPC*, 394, 397
- Pacaud F., et al., 2006, *MNRAS*, 372, 578
- Pierre M., et al., 2004, *JCAP*, 9, 11
- Pierre M., et al., 2007, *MNRAS*, 382, 279 (Paper I)
- Ueda Y., et al., 2008, *ApJS*, 179, 124
- Watson M. G., et al., 2009, *A&A*, 493, 339
- Willis J.P., et al., 2012, submitted to *MNRAS*

## APPENDIX A: LISTINGS OF DATABASE CONTENT

The list of columns in the X-ray single-band and band-merged tables is almost the same as in Paper I, however is reported for completeness in Tables A1 and A2. As for Paper I, the *main* parameters (as flagged in such tables) of the merged X-ray catalogue will be available in electronic form also at the CDS. The multiwavelength tables have instead a substantially increased number of columns, which are listed in Table A3.

## APPENDIX B: DETAILS OF PROBABILITY COMPUTATION

Probabilities of chance association between a counterpart and an X-ray source are computed using formula (1) in Section 4.3, where the density  $n(\text{brighter than } m)$  is computed from simple linear fits as reported in Table B1. The same table indicates also the magnitudes or fluxes used to look-up at the density for the appropriate band. We did only a rough estimate of the parametrization of the density for the entire XMM-LSS area, neglecting any possible spatial variation.

X-ray to CFHTLS probability, called `probX0`, is computed for sources with a CFHTLS counterpart in the order: D1 if present, else W1. In the case of undefined CFHTLS magnitudes, the pointing tile limiting magnitude was used (read directly from the W1 table, or fixed to  $i' = 25$  for D1).

The other probabilities, X-ray to SWIRE probability `probXS`, X-ray to UKIDSS probability `probXU`, and X-ray to GALEX probability `probXG`, are computed as given in the notes in Table B1.

A probability of 99 ("undefined") is assigned whenever it could not be computed.

A statistics of the probability ranking defined in Section 4.3 is shown in Fig. B1. This figure indicates an acceptable tuning with the CFHTLS, SWIRE and UKIDSS catalogues, while GALEX data are perhaps *overtuned* in the sense that there is an excess of good probabilities. This may indicate that the probability computation has to be revised.

## APPENDIX C: COMPARISON BETWEEN CATALOGUES

We provide here details on the comparisons: (a) between 2XLSSd and Version I XLSS (Section C1); (b) between 2XLSSOPT and 2XLSSOPTd (Section C2); (c) between our catalogues and the XMDS one (Section C3); (d) between our catalogues and the 2XMM one (Section C4).

### C1 Comparison between XLSS and 2XLSSd

We first checked that the new pipeline version provides results consistent with the previous IDL version by performing detailed tests on simulated and real XMM pointings. The detection parts of both pipelines give nearly identical results for point-like and extended sources. The characterization parts (maximum likelihood fitting) are in excellent agreement for point-like sources. Regarding extended sources, comparison of fluxes, sizes and likelihoods estimates from the two pipelines are in very good agreement. Some differences do however show up for individual faint sources or sources close to the detector borders and gaps. These differences can be attributed to statistical fluctuations, and comparing these values to the input characteristics of simulated sources in a statistical sense, we conclude that both pipelines perform equivalently. Finally we compared directly the results.

The association between sources in the Version 2 catalogues (2XLSS and 2XLSSd) with the earlier XLSS release (in the smaller area covered by the latter) is possible using the database column `XLSSpointer`, as explained in Section 3.5. 2824 sources are common between XLSS and 2XLSSd (out of 3385 in XLSS). There are 452 objects appearing only in 2XLSSd in the pointings covered by XLSS, and 561 XLSS objects not confirmed in 2XLSSd. A majority (respectively 95% of the former and 88% of the latter) have a poor detection likelihood ( $LH < 40$  corresponding conventionally to  $< 3\sigma$ ). As an example of the rather good agreement between the two catalogue versions (mainly between the older and newer XAMIN version, and also between the  $6''$  vs  $10''$  band merging) we compare the fluxes between XLSS and 2XLSSd (which makes sense since XLSS was also using full exposures), via the plots given in Fig. C1.

### C2 Comparison between 2XLSSOPT and 2XLSSOPTd

There are 20837 potential counterpart sets for 6721 X-ray sources in input for 2XLSSOPTd, and 16813 for 5572 sources for 2XLSSOPT (the comparison includes negative rank *rejected* counterparts since rejection may act differently because of the displacement). Of these, 1188 entries (for 428 X-ray sources) in 2XLSSOPT have no obvious correspondent in the deep 2XLSSOPTd.

On the other hand 15625 counterpart sets are associated with 5144 X-ray sources in 2XLSS with a corresponding source in 2XLSSd. These are the X-ray sources present in both catalogues.

13454 counterpart sets (86% of the common ones) for 4979 2XLSS sources (97% of the common ones) are identical (i.e. have the same counterparts in all non-X-ray catalogues).

Of these, 139 are confirmed "blank fields" (no *catalogued* counterpart in any waveband).

Of the remaining 13315, 11556 (87%) have the same rank in 2XLSSOPTd and 2XLSSOPT, namely, with reference to the rank definitions in Section 4.3:

3710 are primary counterparts,

1439 are secondary counterparts,

6407 are rejected counterparts, not included in the catalogues.

1759 (of the 13315) have the same counterpart but with a different rank:

for 511 of them the rank change is irrelevant (i.e. they remain anyhow the primary counterpart in both catalogues);

201 and 175 counterpart sets rejected in 2XLSSOPTd are respectively primary and secondary choices in 2XLSSOPT;

170 and 196 primary or secondary in 2XLSSOPTd are rejected in 2XLSSOPT;

254 2XLSSOPTd primaries become secondary in 2XLSSOPT while 252 undergo the opposite change from secondary to primary.

In 38 additional cases (only 0.2% of the common ones) the counterpart set is the same between a couple of 2XLSSOPT and 2XLSSOPTd entries, but the latter are not associated by column `Xdeep`. I.e. two sources have the same counterpart set but are not the closest. In 10 cases this is due to ambiguous band merging, but in the rest (which is anyhow an extremely small number) this probably means that there are two 10 ks sources both displaced from but close to a given full exposure one (or v.v.).

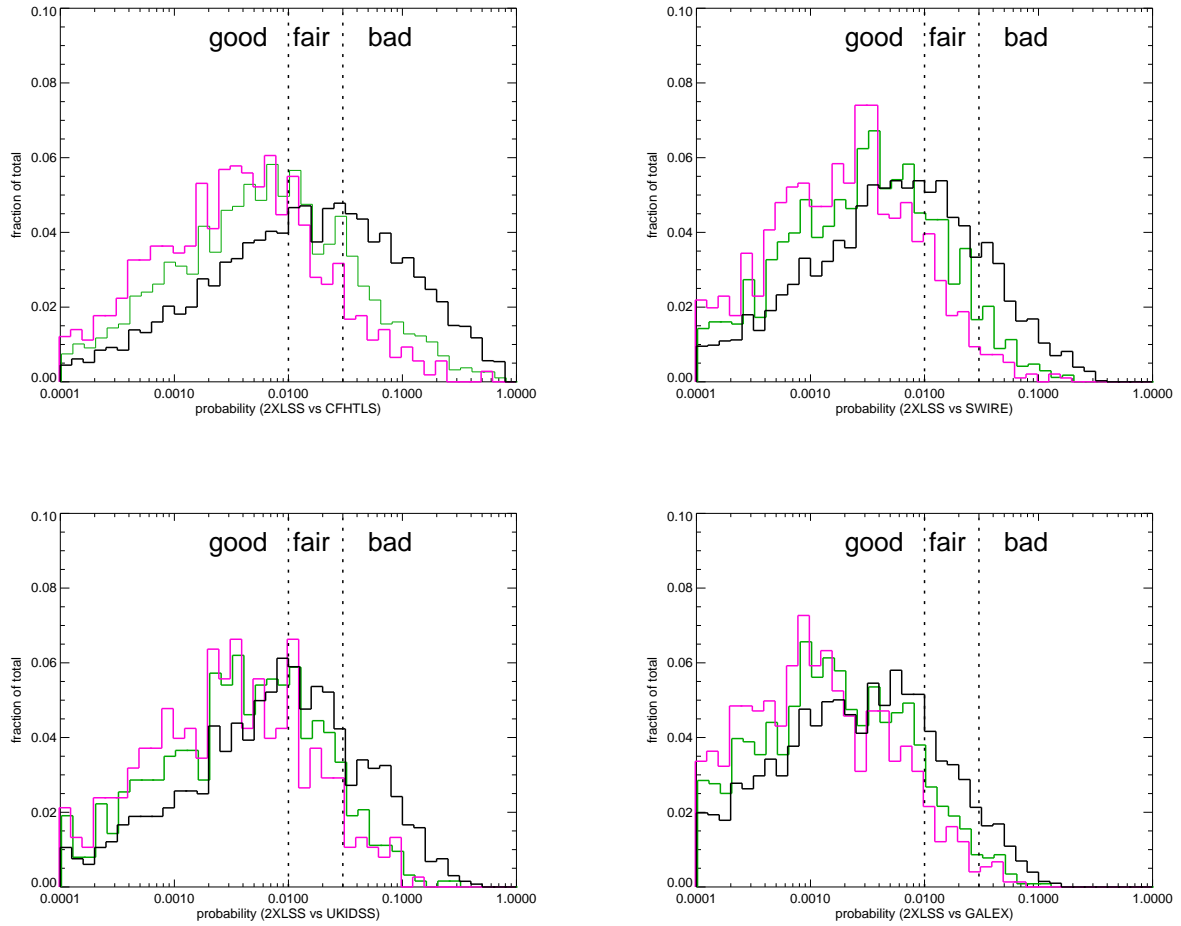


**Figure B1.** Histograms of the four probabilities ( $\text{probX0}$ ,  $\text{probXS}$ ,  $\text{probXU}$  and  $\text{probXG}$ ) normalized to the total number of best counterparts without any undefined probability in the total sample (thick black), with a detection likelihood of at least  $40$  ( $3\sigma$ ) in the best band (thin light gray, green on the web version), or of at least  $75$  ( $4\sigma$ , thick dark gray, magenta on the web version). The dashed fiducial lines identify the loci with good, fair, or bad probability as defined in Section 4.3.

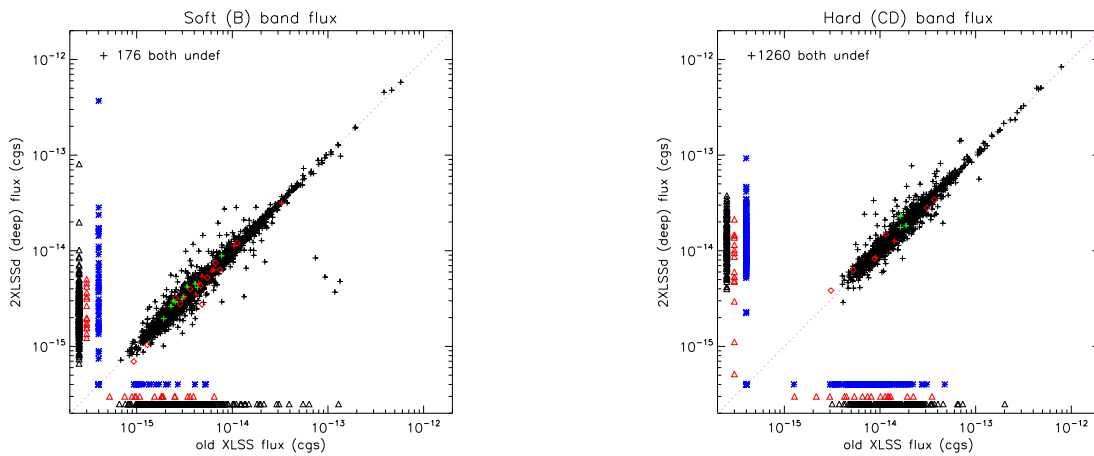


**Figure C1.** Comparison of the flux in the soft (left column) and hard (right column) energy bands between the Version I XLSS catalogue and 2XLSSd. Symbols are identical to those of Fig. 6.

**Table A1.** List of parameters provided in the public XMM-LSS catalogues. All are available at the XMM-LSS Milan database in the separate tables 2XLSSB or 2XLSSBd for the soft band and 2XLSSCD or 2XLSSCDd for the hard band. The column name has an appropriate prefix: when there are two column names given, one with the prefix B and one with the prefix CD, only the one applicable to the given band appears in the relevant table but both may show up in the band-merged tables 2XLSS or 2XLSSd (the family of tables 2XLSSd, 2XLSSBd and 2XLSSCDd constitutes the full exposure catalogue, while 2XLSS, 2XLSSB and 2XLSSCD the 10 ks one); column names without prefix are relevant to the individual band only. The last four columns indicate respectively: (X) whether a parameter is natively computed by XAMIN; (m) whether a parameter is available also in the band-merged table; (o) whether a parameter is present in the multiwavelength table together with those described in Table A3; and (C) whether a parameter is present in the catalogue stored at CDS.

Column name	units	meaning and usage	X	m	o	C
Bseq or CDseq	–	internal sequence number (unique)	X	X	X	
Bcatname or CDcatname	–	IAU catalogue name 2XLSS $x$ Jhhmmss.s-ddmmss, $x$ =B or CD	X	X	X	
Xseq	–	numeric pointer to merged entry see Table A2	X	X	X	
Xcatname	–	name pointer to merged entry see Table A2	X	X	X	
Xlsspointer	–	Xseq of corresponding source in XLSS version I catalogue	X	X	X	
Xdeep	–	Xseq of corresponding source in 2XLSSd (in table 2XLSS only)	X	X	X	
Xfield	–	XMM pointing number (internal use)	X	X		
FieldName	–	XMM pointing name	X	X		
Xbadfield	0 or 1	pointing is good (0) or bad (1)		X	X	
expm1	s	MOS1 camera exposure in the band	X			
expm2	s	MOS2 camera exposure in the band	X			
exppn	s	pn camera exposure in the band	X			
gapm1	"	MOS1 distance to nearest gap	X			
gapm2	"	MOS2 distance to nearest gap	X			
gappn	"	pn distance to nearest gap	X			
Bnearest or CDnearest	"	distance to nearest detected neighbour	X	X		
Bclc2	0–1–2	1 for class C1, 2 for C2, 0 for undefined		X	X	X
CDclc2	0–1–2	1 for class C1, 2 for C2, 0 for undefined				
Bcorerad or CDcorerad	"	core radius EXT (for extended sources)	X	X		X
Bextlike or CDextlike	–	extension likelihood EXT_LH	X	X		X
Bdetlik_pnt or CDdetlik_pnt	–	detection likelihood DET_LH for point-like fit	X			
Bdetlik_ext or CDdetlik_ext	–	detection likelihood DET_LH for extended fit	X			
Boffaxis or CDoftaxis	'	off-axis angle		X		X
Brawra_pnt or CDrawra_pnt	°	source RA (not astrometrically corrected) for point-like fit	X			
Brawdec_pnt or CDrawdec_pnt	°	source Dec (not astrometrically corrected) for point-like fit	X			
Brawra_ext or CDrawra_ext	°	source RA (not astrometrically corrected) for extended fit	X			
Brawdec_ext or CDrawdec_ext	°	source Dec (not astrometrically corrected) for extended fit	X			
Bra_pnt or CDra_pnt	°	source RA (astrometrically corrected) for point-like fit	X			
Bdec_pnt or CDdec_pnt	°	source Dec (astrometrically corrected) for point-like fit	X			
Bra_ext or CDra_ext	°	source RA (astrometrically corrected) for extended fit	X			
Bdec_ext or CDdec_ext	°	source Dec (astrometrically corrected) for extended fit	X			
Bposerr or CDposerr	"	error on coordinates according to Table 4		X		X
Bratemos_pnt or CDratemos_pnt	ct/s	MOS count rate for point-like fit	X			
Bratepn_pnt or CDratepn_pnt	ct/s	pn count rate for point-like fit	X			
Bratemos_ext or CDratemos_ext	ct/s	MOS count rate for extended fit	X			
Bratepn_ext or CDratepn_ext	ct/s	pn count rate for extended fit	X			
countmos_pnt	ct	MOS number of counts for point-like fit	X			
countpn_pnt	ct	pn number of counts for point-like fit	X			
countmos_ext	ct	MOS number of counts for extended fit	X			
countpn_ext	ct	pn number of counts for extended fit	X			
bkgmos_pnt	ct/pixel/detector	MOS local background for point-like fit	X			
bkgpn_pnt	ct/pixel	pn local background for point-like fit	X			
bkgmos_ext	ct/pixel/detector	MOS local background for extended fit	X			
bkgpn_ext	ct/pixel	pn local background for extended fit	X			
Bflux or CDflux	erg/cm <sup>2</sup> /s	source flux (undefined i.e. -1 for extended)		X		X
Bfluxflag or CDfluxflag	0 to 2	0 if MOS-pn difference < 20%, 1 between 20%-50%, 2 above 50%		X		X

The 2171 remaining 2XLSSOPT counterpart sets (covering 1479 individual 2XLSS X-ray sources) can be *altogether different* from all counterpart sets in 2XLSSOPTd for the associated X-ray source (the X-ray source position moved so much that entire counterpart sets are farther than 6'' from either position), or may partially match (from 1 to 4 out of the 5 D1, W1, SWIRE, UKIDSS or GALEX catalogues).

A breakdown of the partial matches (with a total larger than

2171, because one specific counterpart set is compared with all the 2XLSSOPTd counterpart sets for the corresponding X-ray source) is:

2150 are no matches,  
 234 cases match in 1 catalogue,  
 66 cases match in 2 catalogues,  
 25 in 3,  
 7 in 4.

**Table A2.** List of database parameters, as Table A1, but for the additional columns present only in the merged catalogue tables 2XLSS or 2XLSSd. When there are two column names given, one with the prefix B and one with the prefix CD, they relate to the given band, and both show up in the band-merged table. Column names with the prefix X are relevant to merged properties.

Column name	units	meaning and usage	X	m	o	C
Xseq	–	Internal sequence number (unique)		X	X	X
Xcatname	–	IAU catalogue name 2XLSSd Jhhmss.s-ddmssc, see Section 3.5		X	X	X
Bspurious and CDspurious	0 or 1	set to 1 when soft/hard component has DET_LH < 15		X		
Bdetlike and CDdetlike	–	detection likelihood EXT_LH (pnt or ext according to source class)	X	X		X
Xra	°	source RA (astrometrically corrected) (pnt or ext acc. to source class in best band)		X	X	X
Xdec	°	source Dec (astrometrically corrected) (pnt or ext acc. to source class in best band)		X	X	X
Bra and CDra	°	source RA (astrometrically corrected) (pnt or ext according to source class)		X	X	X
Bdec and CDdec	°	source Dec (astrometrically corrected) (pnt or ext according to source class)		X	X	X
Xbestband	2 or 3	band with highest likelihood: 2 for B, 3 for CD		X		
Xastrocorr	4 or 5	astrometric correction from CFHTLS (4) or USNO (5) or none (0)		X		
Xmaxdist	"	distance between B and CD positions		X		
Xlink	–	pointer to Xseq of secondary association, see Section 3.5		X		
Bratemos and CDratemos	ct/s/detector	MOS count rate (pnt or ext according to source class)	X	X		X
Bratepn and CDratepn	ct/s	pn count rate (pnt or ext according to source class)	X	X		X

An alternative breakdown (totalling 2171) is the following:

- 261 single no-match cases,
- 1601 multiple no-matches per X-ray source,
- 15 cases with one counterpart set with 1-3 matches,
- 51 cases with one no-match and one 1-3 matches,
- 6 cases with mixed matches,
- 237 with more no-match and mixed matches.

A different approach for the comparison is to consider only the *best counterparts* i.e. those ranked 0-1 (by definition one per X-ray source). Let us exclude the 1607 2XLSSOPTd (24% of 6721) X-ray sources not confirmed in the 10ks catalogue, and the 528 2XLSSOPT (8% of 5572) new in the 10ks catalogue, and let us concentrate on the common sources. Of their best counterparts:

≈ 86% are essentially confirmed in both catalogues, namely

- 3% are confirmed tentative blank fields,
- 72% have the same counterparts and the same rank,
- 10% have the same counterparts and compatible ranks,
- only 1.4% have partially matching counterpart sets with the same or compatible best rank.

A further 5% and 4% have the same counterparts but they are ranked differently (the best counterpart in one catalogue is either secondary or rejected in the other).

The remaining 5% have altogether different or partially matching counterparts which are ranked differently.

*So the difference between counterparts in the deep and 10ks catalogues is confined to less than 15% of the common sources.*

### C3 Comparison with XMDS

A subset of the XMDS (*XMM* Medium Deep Survey) data was published as the XMDS/VVDS  $4\sigma$  catalogue (Chiappetti et al. 2005; the same paper contained also the logN-LogS of the entire catalogue). Contextually to the release of the entire XMDS catalogue through our database contextually with Version 2 *XMM*-LSS ones (see Table 2), we report here some details of a comparison between the catalogues presented in this paper (mainly 2XLSSd) and XMDS.

The main procedural differences between the two pipelines can be summarized as follows:

- (i) The XMDS covers the fields G01 to G19 in Table 1
- (ii) XMDS data were analysed with a *fully independent* (and more traditional) pipeline based on the one by Baldi et al. (2002).
- (iii) The XMDS pipeline uses the SAS to detect candidates in 5 energy bands simultaneously (and not in 2 independent bands with later merging) operating on event files merged from all 3 *XMM* cameras and from the entire *XMM* field of view (not just the central 13'),
- (iv) It then applies the Baldi et al. (2002) characterization, which is robust but oriented to point sources only (unlike the wavelet method in XAMIN which handles better extended sources).
- (v) The event pattern selection is different (non-standard and broader in XMDS).
- (vi) The removal of redundant sources is handled differently, in particular the primary detection is chosen differently, the position is inherited from the primary detection, but the flux is obtained stacking data from all overlapping pointings.
- (vii) The astrometric correction offsets are different.
- (viii) Also the XMDS catalogue does not include spurious objects (but only those above a probability threshold), so the difference between the raw database table and the catalogue is only due to the overlap removal procedure.

#### C3.1 Comparison of the X-ray source lists

As anticipated in Section 5.3, the XMDS catalogue includes 1168 sources, by definition all in the G-labelled fields. Comparison with the 2XLSSd or 2XLSS catalogues may also involve adjacent B fields if the *XMM*-LSS overlap removal procedure preferred those. The association between XMDS and *XMM*-LSS sources is done within a radius of  $10''$ . The comparison occurs naturally with the deep catalogue, because it involves the *same* input (ODF) event data (for the full exposures) with different pipelines and procedures. Of those 1168 objects:

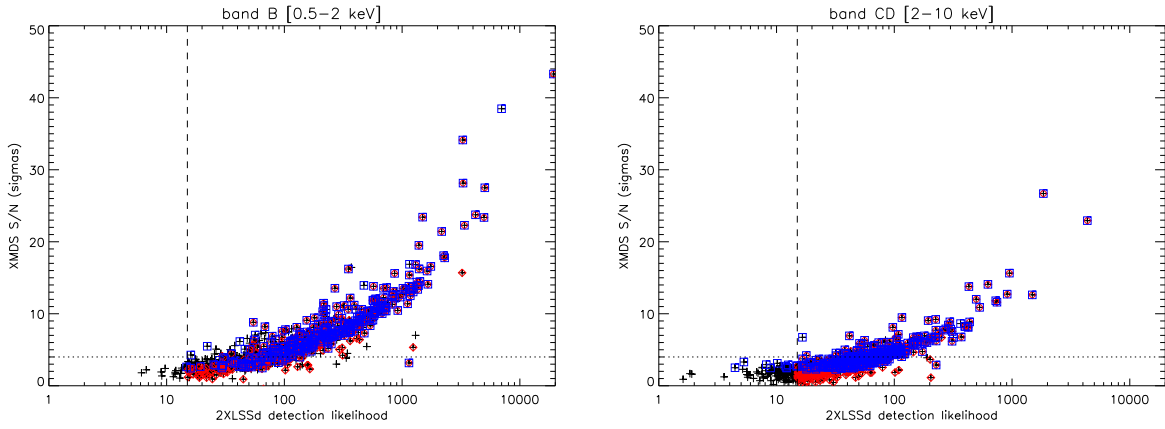
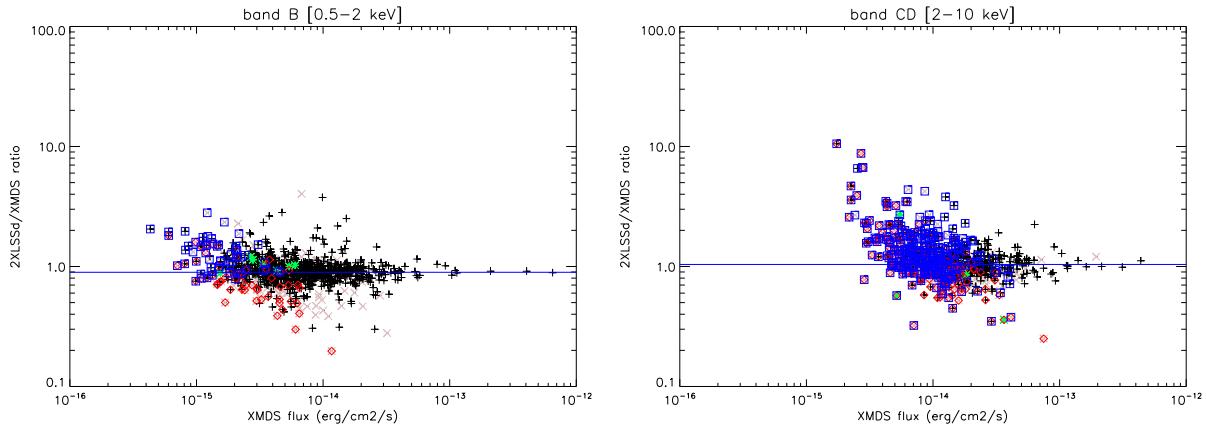
- 1082 have a counterpart in the full exposure input tables,
- of which 1057 are catalogued in 2XLSSd;

**Table A3.** List of additional non-X-ray columns in the multiwavelength 2XLSSOPT or 2XLSSOPTd tables: they also include columns with the X, B or CD prefixes from Tables A1 and A2, while those with the O, S, U or G prefix refer to optical, SWIRE, UKIDSS or *GALEX* data, and those without prefix to combined properties.

Column name	units	meaning and usage
Xrank	-1 0 1 2	ranking of the counterpart set (see 4.3)
Ou	magnitude	$u^*$ magnitude
Og	magnitude	$g'$ magnitude
Or_	magnitude	$r'$ magnitude
Oi	magnitude	$i'$ magnitude
Oz	magnitude	$z'$ magnitude
Ou_e	magnitude	error on $u^*$ magnitude
Og_e	magnitude	error on $g'$ magnitude
Or_e	magnitude	error on $r'$ magnitude
Oi_e	magnitude	error on $i'$ magnitude
Oz_e	magnitude	error on $z'$ magnitude
OseqD1	–	internal sequence number (if magnitudes from D1 field)
OseqW1	–	internal sequence number (in W1 or ABC fields)
Ofield	–	CFHT field identification in form $\pm x \pm y$ or D1 or A,B,C (see 4.1 and Fig. 1)
Ora	°	RA of the optical candidate
Odec	°	Declination of the optical candidate
Oflag	–	binary flag combining 0/1 galaxy/star, 0/4 normal/masked, 0/8 normal/saturated
Sf36	$\mu\text{Jy}$	IRAC flux at 3.6 $\mu\text{m}$
Sf45	$\mu\text{Jy}$	IRAC flux at 4.5 $\mu\text{m}$
Sf58	$\mu\text{Jy}$	IRAC flux at 5.8 $\mu\text{m}$
Sf80	$\mu\text{Jy}$	IRAC flux at 8.0 $\mu\text{m}$
Sf24	$\mu\text{Jy}$	MIPS flux at 24 $\mu\text{m}$
Sf70	$\mu\text{Jy}$	MIPS flux at 70 $\mu\text{m}$
Sf160	$\mu\text{Jy}$	MIPS flux at 160 $\mu\text{m}$
Sf36_e	$\mu\text{Jy}$	error on 3.6 $\mu\text{m}$ flux
Sf45_e	$\mu\text{Jy}$	error on 4.5 $\mu\text{m}$ flux
Sf58_e	$\mu\text{Jy}$	error on 5.8 $\mu\text{m}$ flux
Sf80_e	$\mu\text{Jy}$	error on 8.0 $\mu\text{m}$ flux
Sf24_e	$\mu\text{Jy}$	error on 24 $\mu\text{m}$ flux
Sf70_e	$\mu\text{Jy}$	error on 70 $\mu\text{m}$ flux
Sf160_e	$\mu\text{Jy}$	error on 160 $\mu\text{m}$ flux
Sseq	–	internal sequence number for SWIRE objects
Sra	°	RA of the SWIRE candidate
Sdec	°	Declination of the SWIRE candidate
Uj	magnitude	J magnitude
Uh	magnitude	H magnitude
Uk	magnitude	K magnitude
Uj_e	magnitude	error on J magnitude
Uh_e	magnitude	error on H magnitude
Uk_e	magnitude	error on K magnitude
Useq	–	internal sequence number for UKIDSS objects
Ura	°	RA of the UKIDSS candidate
Udec	°	Declination of the UKIDSS candidate
Gnuv	mJy	<i>GALEX</i> near UV flux
Gfuv	mJy	<i>GALEX</i> far UV flux
Gnuv_e	mJy	error on near UV flux
Gfuv_e	mJy	error on far UV flux
Gseq	–	internal sequence number for <i>GALEX</i> objects
Gra	°	RA of the <i>GALEX</i> candidate
Gdec	°	Declination of the <i>GALEX</i> candidate
distXO	"	distance from the X-ray corrected position to the optical position
distXS	"	distance from the X-ray corrected position to the SWIRE position
distXU	"	distance from the X-ray corrected position to the UKIDSS position
distXG	"	distance from the X-ray corrected position to the <i>GALEX</i> position
probXO	–	chance probability of X-ray to optical association (see 4.3)
probXS	–	chance probability of X-ray to SWIRE association (see 4.3)
probXU	–	chance probability of X-ray to UKIDSS association (see 4.3)
probXG	–	chance probability of X-ray to <i>GALEX</i> association (see 4.3)

**Table B1.** Parameters used for probability computation.

Probability	$m$	density $n(\text{brighter than } m)$	a	b	Notes
$probXO$	$i'$	$n(< i') = 10^{a+bi'}$	-9.32415	0.293833	for D1 field
			-9.23183	0.290519	for W1 excluding ABC fields
$probXS$	$r'$	$n(< r') = 10^{a+br'}$	-9.18619	0.279706	for W1 ABC fields
	$F_\lambda$	$n(> F_\lambda) = 10^{a+b*\log(F_\lambda)}$			in increasing order of $\lambda$ whichever first
	$\lambda = 3.6\mu\text{m}$		-1.68062	-0.944191	
	$\lambda = 4.5\mu\text{m}$		-1.73693	-0.976644	
	$\lambda = 5.8\mu\text{m}$		-2.04933	-0.829700	
	$\lambda = 8.0\mu\text{m}$		-1.49944	-1.07201	
	$\lambda = 24\mu\text{m}$		0.102480	-1.53410	
$probXU$	$J$	$n(< J) = 10^{a+bJ}$	-8.67503	0.268272	taken best if both bands are present
	$K$	$n(< K) = 10^{a+bK}$	-8.96264	0.321560	
$probXG$	$NUV$	$n(< NUV) = 10^{a+bNUV}$	-11.0875	0.326965	taken best if both bands are present
	$FUV$	$n(< FUV) = 10^{a+bFUV}$	-13.9827	0.433838	

**Figure C2.** Cross calibration between the 2XLSSd (XAMIN) detection likelihood and the XMDS signal to noise ratio. Left panel for the soft band, right panel for the hard band. The dashed vertical line indicates the 2XLSSd acceptance thresholds of  $LH > 15$ , while the dotted horizontal line shows the conventional level of  $4\sigma$ . Crosses indicate all objects detected in the given band. A (red) diamond surrounds the sources detected above LH threshold *in both bands* in 2XLSSd, while a (blue) square surrounds those detected above the chance probability threshold *in both bands* in the XMDS.**Figure C3.** The ratio of the 2XLSSd and XMDS fluxes as a function of the XMDS flux for band B (left panel) and band CD (right panel). The horizontal solid line is a fiducial line corresponding to the actual average ratio in the band (see text). The (black) crosses indicate point-like sources which have a `fluxflag` of 0 or 1, the (pink) X those with a `fluxflag` of 2, i.e. where the MOS and pn fluxes differ by more than 50%. The (green) asterisks correspond to extended C2 sources for which the flux is computed from the point-like rates (C1 sources have flux set to undefined and are not plotted). A (red) diamond surrounds the points with a poor 2XLSSd likelihood  $15 < LH < 20$  in the band. A (blue) square surrounds the points with a poor XMDS probability  $prob > 2 \times 10^{-4}$  in the band. Note that the latter symbols are different from those used in Fig. C2.

while 1019 have one in the 10 ks input tables, of which 956 in 2XLSSd.

Of the 86 XMDS sources not in the input table for 2XLSSd:

23 are at off-axis angles greater than  $13'$  (ignored by XAMIN), and 39 anyhow at large off-axis angles ( $> 10'$ ), so it is not surprising they were excluded by XAMIN;

similarly 43 are potential ultrasoft sources (the band with the highest S/N ratio in XMDS is the A band [0.3-0.5 keV], which is not processed by the current release of XAMIN), so they are legitimately excluded;

considering the XMDS significance, 46 and 72 are respectively below  $3\sigma$  and  $4\sigma$ ;

if one allows the combination of different conditions, a net majority of the XMDS-only sources (76) are *either* ultrasoft, or at off-axis  $> 10'$  or at  $< 3\sigma$ .

We concentrate below on the 1057 XMDS sources with a 2XLSSd correspondent (which can be called *common catalogued*). Of them:

783 are in the same (G) field, so should be exactly the same detections;

173 are stacked XMDS entries;

the remaining 103 cases associate sources detected in different pointings: 39 in another G field, 64 in a B field.

Concerning the distance between the (astrometrically corrected) X-ray positions in the XMDS and 2XLSSd catalogues, 58% of the sources are closer than  $2''$ , 88% closer than  $4''$  and only 4% more distant than  $6''$ , in general concentrated among the sources with lesser significance, and the few extended ones. The agreement between XMDS and 2XLSSd positions, peaking around  $1''$ , is better than the typical inter-band distance between 2XLSSd detections in the two energy bands, which peaks around  $2''$ . Compare panels (d) and (c) of Fig. 5.

We have cross calibrated graphically the detection likelihood of XAMIN with the chance probability of the XMDS (for definition see Baldi et al. 2002) and the detection likelihood of XAMIN with the significance in terms of number of  $\sigma$  of the XMDS (see Chiappetti et al. (2005) and references therein). We only show the latter in Fig. C2. One can see that a likelihood of 75 corresponds more or less to the  $4\sigma$  level, and one of 40 to the  $3\sigma$  level.

We also note that 89% of the common sources have B as the best band (highest likelihood) in 2XLSSd. To be more precise:

96% of the sources are observed by 2XLSSd in the B band,  
62% are observed in the CD band, and  
57% are observed in both.

This can be compared with the totality of the 2XLSSd catalogue, where (with no appreciable difference between the full 2XLSSd catalogue and the sources in the G fields alone):

84% of the sources have B as the best band,  
89% are observed in the B band,  
48% in the CD band, and  
37% in both.

The XMDS by construction includes measurements in all 5 energy bands even if the source is above the probability threshold only in one. If we consider as good detections for XMDS only those with  $prob < 2 \times 10^{-4}$  in the band, we have that, of the sources in common with 2XLSSd:

91% are detected in the B band,

36% in the CD band, and  
30% in both.

The fluxes, computed for XMDS according to the prescriptions of Baldi et al. (2002) and for XMM-LSS as explained in Section 3.1.1, are compared in Fig. C3. Extended sources classified C1 are excluded as their 2XLSSd flux is set to undefined. The fluxes match qualitatively, although there is a systematic difference: namely 2XLSSd fluxes are 0.895 lower than the XMDS fluxes in the B band, while they are only 1.040 higher in the CD band.

It can be seen that a larger scatter in fluxes occurs for the sources which have poorer significance in either catalogue, while outliers are generally due to sources presumably falling near a chip gap on one detector (and as such characterized by a `fluxflag` of 2), or exceptionally by residual C2 extended sources (for which the XMM-LSS flux is computed from the point-like rate).

### C3.2 Comparison of the optical counterparts

It is also possible, similarly to what was done in Section 5.2.2, to compare the counterparts in optical (and other) bands between the XMDS catalogue and one of our XMM-LSS catalogues. In doing this one should consider:

(i) that the identification procedure for XMDS is historically different from the one used here, in particular it was done in several incremental steps, and uses distances capped to  $2''$  in the computation of probabilities,

(ii) that the catalogues used for XMDS were in larger number (for a total of 27) and included many other, including older, data sources (e.g. VVDS, radio data, SIMBAD and NED, CFHTLS T003, etc.)

Therefore we present a comparison limited to the 2XLSSOPTd catalogue (the one which matches better XMDS in exposures), and, for XMDS, to *reduced counterpart sets* considering only CFHTLS T004 D1 and W1, SWIRE DR6 and GALEX. UKIDSS was not included since 2XLSSOPTd uses release DR5, while XMDS used release DR3. More specifically we consider only the 1057 X-ray sources in common between XMDS and 2XLSSd, as described in C3.1.

They correspond to 4316 counterpart sets (of any rank) in 2XLSSOPTd and 4916 in XMDS. We found that a large fraction (3620) of the possible counterpart sets are identical (i.e. they have the same counterparts, irrespective of ranking, in both catalogues).

We can then concentrate on the *best counterparts* (ranks 0-1; a similar ranking system, though different in details, was used also for XMDS):

for 627 cases (59% of 1057) the best counterpart is exactly the same in all 4 D1, W1, SWIRE and GALEX catalogues,  
for 16% in 3 catalogues (the other may be different or missing),  
for 15% in 2,  
for 4% in 1;

making a total of 81% with the choice of a highly compatible counterpart.

A very limited number of cases (5 and 8) are potential "blank fields" respectively in 2XLSSOPTd and XMDS, with another counterpart in the other catalogue.

The remaining 193 (18%) cases select an altogether different counterpart in the two catalogues:

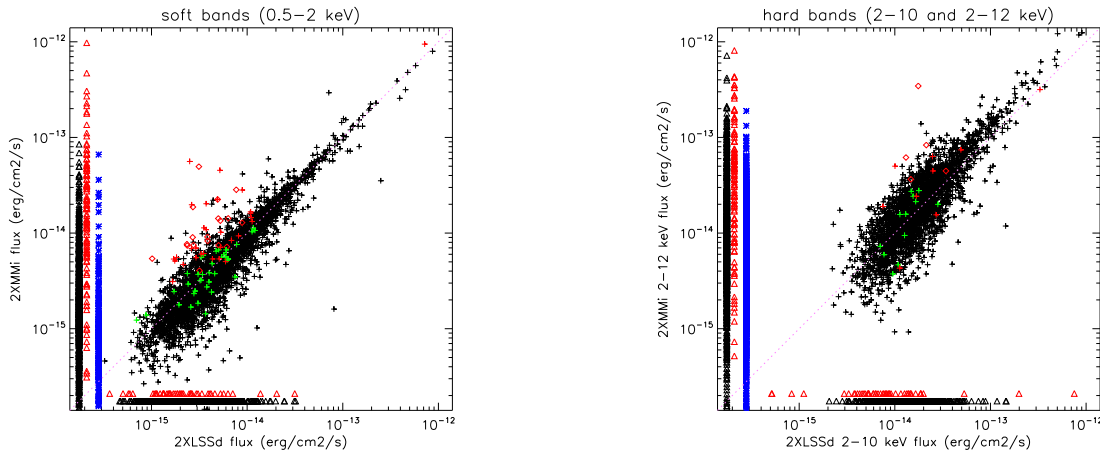


**Figure C4.** Comparison of the flux in the soft (left panel) and hard (right panel) energy bands, between 2XLSSd and 2XMM. Crosses and diamonds indicate point-like or extended objects associated in the two catalogues (see text). Blue asterisks indicate fluxes present but *undefined* in 2XLSSd, while triangles indicate sources present only in one catalogue (both are placed at a conventional out-of-range X or Y coordinate). Colour coding (only in the web version) is as follows: black cross for point-like common sources, red diamond for extended sources in both 2XLSSd and 2XMM, green cross for 2XLSSd extended object point-like in 2XMM; vice versa for red cross; triangles are black or red for point-like or extended sources. Remember that fluxes for C1 extended sources are undefined in our database (see Table 9 in Paper I).

for 97 2XLSSOPTd and 77 XMDS sources the counterpart set is present only in one catalogue and fully replaced by something else in the other;

in other 96 or 116 cases, the counterpart set which is preferred in one catalogue is still present in the other with a different rank (secondary or rejected).

In conclusion, the compatibility between the counterparts is satisfactory.

#### C4 Comparison with 2XMM

We quickly compared our 2XLSSd catalogue with the 2XMM catalogue (Watson et al. 2009). Namely we used the 2XMMi-DR3 “slim” reduced catalogue<sup>13</sup>, which contains exposure-merged sources (not individual detections), and thus somewhat compare with our post overlap-removal catalogues.

We restricted a comparison to a rectangular area fully encompassing 2XLSSd and noticed that such an area includes precisely just our pointings, with the only exception of a single additional pointing centered on the bright star Mira Ceti (ObsId 014850 0201).

The rectangular area contains 6181 2XMM sources. Since the slim catalogue does not contain indication on the pointings, we can tentatively flag sources in the Mira Ceti field as the 60 within 13' from the respective pointing centre. We checked the association with our 6721 2XLSSd sources within the customary radius of 10". We find:

- 5039 sources are associated
- 1682 2XLSSd ones are not associated
- 1141 2XMM ones are not associated

We note that 59% of the unassociated 2XLSSd sources have a rather poor likelihood ( $ML < 20$ ), and 93% are below  $ML < 40$  (i.e.  $3\sigma$ ). Despite the different definition of the 2XMM likelihood

(parameter SC\_DET\_ML), we note that of 1141 unassociated 2XMM sources, 67% have SC\_DET\_ML < 15.

Of the associated cases, all but 69 have a single association. The ambiguous ones are all plain couples, and usually well separated (one 2XMM source at 1-2" from the 2XLSSd position, and the other at 8-9").

The distance between the astrometrically corrected position (2XMM used the USNO catalogue for this purpose) for the associated primary (closest) cases is within 2" in 55% of the cases, within 4" in 86% and within 6" in 95% (while 90% of the 69 secondaries are above 6"). The histogram of distances however peaks at a 1" offset (not unlike XMDS vs 2XLSSd).

The common subset contains 100 of our extended sources, and 88 2XMM extended sources (i.e. those with their parameter SC\_EXTENT > 0). 56 are considered extended in both catalogues. 110 of our extended sources do not appear at all in 2XMM, and 113 2XMM extended sources do not appear in 2XLSSd.

The 2XMM slim catalogue does not contain count rates. It contains fluxes in several energy bands, but these are different from ours. We can directly compare the sum of 2XMM bands 2 and 3 with our B band (0.5-2 keV), while at harder energies we can compare the sum of 2XMM bands 4 and 5 (2-12 keV) with our CD band (2-10 keV).

The comparison of the fluxes is reported in Fig. C4. The average 2XMM/2XLSSd flux ratio for common point-like sources is 0.92 in the soft band (same energy range), and 1.22 in the hard bands (where 2XMM extends 2 keV further). Again, considering the differences in the pipelines, the agreement is acceptable.

This paper has been typeset from a  $\text{\TeX}/\text{\LaTeX}$  file prepared by the author.

<sup>13</sup> [http://xmmssc-www.star.le.ac.uk/Catalogue/2XMMi-DR3cat\\_slim\\_v1.0.csv.gz](http://xmmssc-www.star.le.ac.uk/Catalogue/2XMMi-DR3cat_slim_v1.0.csv.gz)